New Potent Acetylcholinesterase Inhibitors in the Tetracyclic Triterpene Series

Thibault Sauvaître,[†] Mireille Barlier,[†] Denyse Herlem,[†] Nohad Gresh,[§] Angèle Chiaroni,[†] Daniel Guenard,*[,†] and Catherine Guillou*[,†]

Institut de Chimie des Substances Naturelles, Bt 27, CNRS, Avenue de la Terrasse, 91198 Gif-sur-Yvette, France, and Laboratoire de Pharmacochimie Moléculaire et Cellulaire, CNRS FRE 2718, U648 INSERM, Université René Descartes (Paris V), 45 rue des Saints-Pères, 75006 Paris, France

Received May 8, 2007

A new highly selective inhibitor of acetylcholinesterase (AChE) was discovered by high-throughput screening. Compound **1** was synthesized from a natural product, the *N*-3-isobutyrylcycloxobuxidine-F **2**. A new extraction protocol of this compound is described. The hemisynthesis and optimization of **1** are reported. The analogs of **1** were tested in vitro for the inhibition of both cholinesterases (AChE and BuChE). These compounds selectively inhibited AChE. Extensive molecular docking studies were performed with **2** and AChE employing Discover Biosym software to rationalize the binding interaction. The results suggested that ligand **2** binds simultaneously to both catalytic and peripheral sites of AChE.

Introduction

While advances in medicine have increased the life expectancy of the population, the number of people affected by age-related pathologies has also consequently increased. One of the most common afflictions of age is Alzheimer's disease (AD[a]).

AD[1] is a progressive neurodegenerative disorder of the central nervous system (CNS) that is characterized by profound memory impairments, emotional disturbance, and also personality changes. The etiology of this disease is not known. Much effort is devoted to elucidate the relationships among the neuropathological hallmarks of the disease, including extracellular amyloid plaques,[2] intracellular neurofibrillary tangles containing abnormally hyperphosphorylated tau protein,[3] and loss of neurons in the nucleus basalis of Meynert and the hippocampus. AD is characterized by a pronounced alteration of the cholinergic system and other neurotransmitter systems (glutamate and serotonine). The cholinergic hypothesis postulates that memory impairments in patients with AD result from a deficit of cholinergic function in the brain.[4]

Current therapeutic approaches are aimed at (i) limiting the effects of oxidative damage by protecting the nerve cells; (ii) reducing the levels of toxic substances by decreasing the production or aggregation of β-amyloid (Aβ) peptide or increasing its removal by inhibiting the phosphorylation of the tau protein; (iii) activating other neurotransmitter systems to indirectly compensate the cholinergic function deficit; and (iv) restoring the native levels of acetylcholine in the CNS by using acetylcholinesterase (AChE) inhibitors.

With respect to the latter strategy, AChE inhibitors are the major and most developed class of drugs approved for AD symptomatic treatment. These include donepezil (Aricept, Pfizer, Inc., and Eisai Corp.),[5] rivastigmine (Exelon, Novartis),[6] and galanthamine (Reminyl renamed Razadyne, Janssen, and Johnson and Johnson).[7] An NMDA receptor antagonist, memantine (Namenda, Merz Pharma, and Forest Labs)[8] has also been launched on the market. In addition to its catalytic activity, AChE exerts secondary noncholinergic functions,[9,10] related to its peripheral anionic site (PAS),[11,12] in differentiation,[13] cell adhesion,[14,15] and in mediating the processing and deposition of Aβ peptide.[16−19] It was postulated that AChE binds through its peripheral site to the nonamyloidogenic form of Aβ protein acting as a chaperone protein and inducing conformational change to the amyloidogenic form with subsequent amyloid fibril formation.[18,19] In vitro, AChE directly promotes the assembly of Aβ peptide into amyloid fibrils forming stable AChE−Aβ complexes.[17] A renewed interest in the search for AChE inhibitors thus has occurred.

In the continuation of our ongoing research[20] on new dual-binding site AChE inhibitors, we describe herein our efforts to explore the structure−activity relationships of a potent inhibitor **1** (*Ee*AChE IC_{50} = 29 nM) identified by high-throughput screening of our Institut's chemical and natural products libraries. Compound **1** is a triterpene-type steroidal alkaloid (Figure 1).

Interestingly, steroidal alkaloids and triterpenoid alkaloids from *Buxus sempervirens L*,[21,22] *Buxus balearica* Willd,[21,22] *Buxus hyrcana P*,[23] *Buxus paillosa S*,[24] *Sarcococca saligna*,[21,25] *Sarcococca hookerina*,[26] and *Sarcococca coriacea*[27] are known to be inhibitors of butyrylcholinesterase (BuChE; in micromolar range) and weak inhibitors of AChE.

Chemistry

Compound **1** is a triterpene-type steroidal alkaloid synthesized from *N*-3-isobutyrylcycloxobuxidine-F **2** (Figure 1) isolated from *Buxus balearica* Willd using a new extraction protocol. In the previous protocol, *N*-3-isobutyrylcycloxobuxidine-F **2** and *N*-3-benzoylcycloxobuxidine-F **3** were isolated in the same fraction. The separation of these two compounds was difficult and required long, tedious chromatographies and countercurrent separations.[28]

In the new protocol, the crude alkaloids were isolated from a dichloromethane/methanol extract of the air-dried leaves macerated in aqueous ammonia solution. The crude alkaloids were separated at different pH values. The fractions obtained at pH 5.8 were combined, dried, and evaporated to give pure

* To whom correspondence should be addressed. Phone: +33 (0)1 69 82 30 75 (C.G. and D.G.). Fax: +33 (0)1 69 07 72 47 (C.G. and D.G.). E-mail: catherine.guillou@icsn.cnrs-gif.fr (C.G.); daniel.guenard@icsn.cnrs-gif.fr (D.G.).

[†] Institut de Chimie des Substances Naturelles, CNRS.

[§] Laboratoire de Pharmacochimie Moléculaire et Cellulaire, CNRS.

[a] Abbreviations: AChE, acetylcholinesterase; BuChE, butyrylcholinesterase; AD, Alzheimer's disease; Aβ, β-amyloid; CNS, central nervous system; PAS, peripheral anionic site.

10.1021/jm070536w CCC: $37.00
Published on Web 09/29/2007

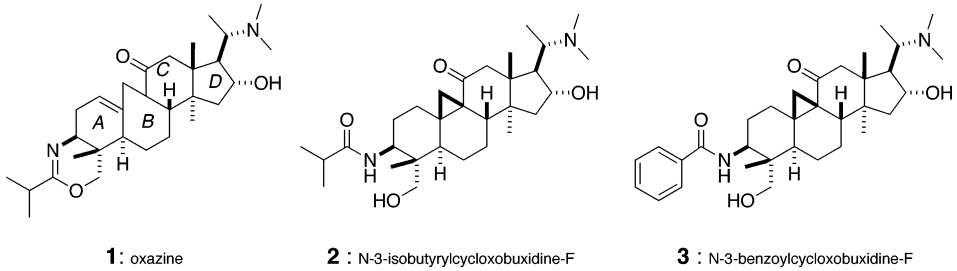

Figure 1. Structures of compounds **1**−**3**.

Scheme 1. Synthesis of Compound **1**[a]

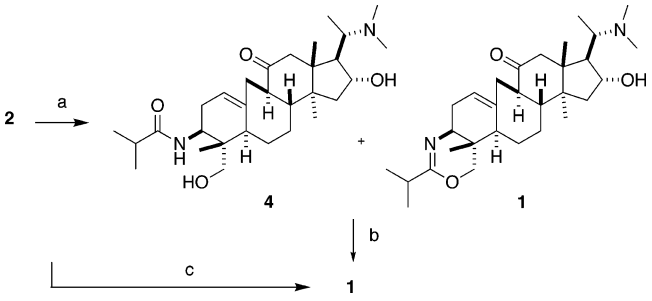

[a] Reagents and conditions: (a) 240 °C, 0.05 mmHg (90%); (b) $Et_4N^+OH^-$, 240 °C, 0.05 mmHg (74%); (c) NaOH (20% mol), ethylene glycol 210 °C (83%).

N-3-isobutyrylcycloxobuxidine-F **2** after trituration with acetone. Compound **2** (100 g) was thus obtained from 11 kg of air-dried leaves.

Compound **1**[29] was first prepared in two steps from **2**. Pyrolysis of **2** at 240 °C under 0.05 mmHg afforded a mixture (82/18) of **1** and **4**, which was then subjected to a second pyrolysis (240 °C, 0.05 mmHg) in the presence of tetraethylammonium hydroxide to yield only **1** (74%). Compound **1** could also be obtained in one step from **2** by heating in ethylene glycol in the presence of sodium hydroxide (83% yield; Scheme 1).

A subsequent single-crystal X-ray diffraction analysis confirmed the structure of compound **1** (Figure 2).

The new 1,3-dihydrooxazines **9a**−**i** were synthesized from cycloxobuxidine-F **5** obtained by hydrolysis of *N*-3-isobutyrylcycloxobuxidine-F **2** (Scheme 2).[30] Preparation of amides **7a**−**i** was carried out by coupling the appropriate anhydrides **6a**−**i** with cycloxobuxidine-F **5**. All anhydrides were readily obtained following the reported methodology,[30] except **6a**−**c** and **6f**, which were commercially available. Subsequent pyrolysis of **7a**−**i** under reduced pressure afforded mixtures of 1,3-dihydrooxazines **9a**−**i** (minor) and compounds **8a**−**i** (major) having an open cyclopropane ring. These resulting mixtures were finally converted into the corresponding 1,3-dihydrooxazines **9a**−**i** by heating under the above conditions in the presence of tetraethylammonium hydroxide (Scheme 2). The mixtures of 1,3-dihydrooxazines **9a**−**i** (minor) and compounds **8a**−**i** (major) were purified on alumina to give compounds **8a**−**i**; during this process, 1,3-dihydrooxazines **9a**−**i** were hydrolyzed to compounds **8a**−**i**.

The 1,3-oxazinane derivatives with cyclopropane and open cyclopropane rings were synthesized following the reactions depicted in Schemes 3 and 4 using compounds **5** and **11** as key intermediates, which were converted into the corresponding 1,3-oxazinanes **10** and **12** by reaction with isobutyraldehyde.

An isomer of **1** that possesses an α,β-ethylenic ketone function (i.e., **14**, instead of **1**, which contains an γ,δ-ethylenic ketone function) was obtained by reaction of **2** with $BF_3{\cdot}OEt_2$ and subsequent cyclization in the presence of tetraetylammonium hydroxide at 300 °C under reduced pressure (Scheme 5).

The syntheses of analogs with modified D rings are shown in Schemes 6 and 7.

Thus, treatment of **1** with acetyl or pivaloyl chloride and pyridine gave the corresponding acetate **15** and pivalate **16** (Scheme 6).

The synthesis of the *N*-demethylated analog of **1** (i.e., **19**) was achieved following the strategy summarized in Scheme 7. *N*-3-Isobutyrylcycloxobuxidine-F **2** was converted into its *N*-oxide **17** by oxidation with *m*-chloroperbenzoic acid. Subsequent treatment of **17** with a mixture of ferrous sulfate heptahydrate[31] and iron chloride hexahydrate provided *N*-demethylated *N*-3-isobutyrylcycloxobuxidine-F **18**, which was then submitted to pyrolysis (240 °C) at 0.03 mmHg to give **19**.

Synthetic routes to tetrahydropyrimidine analogs of 1,3-dihydrooxazines **26a**,**b** and **33** were also developed (Schemes 8 and 9). The 16-hydroxy function was first protected as an acetate (i.e., **20a**,**b**, **27**). Oxidation of the alcohol group at position 29 with Dess−Martin-periodinane afforded the corresponding aldehydes (i.e., **21a**,**b**, **28**). Subsequent deprotection of the hydroxy function furnished **22a**,**b** and **29**, which were submitted to reductive amination to give benzylamines **24a**,**b** and **31**. The benzyl group was then removed by hydrogenolysis of **24a**,**b** and **31** with ammonium formate as hydrogen donor and palladium on charcoal to afford amines **25a**,**b** and **32**. Treatment of the terminal amines with triethylamine in *n*-butanol provided the expected pyrimidines **26a**,**b** and **33**.

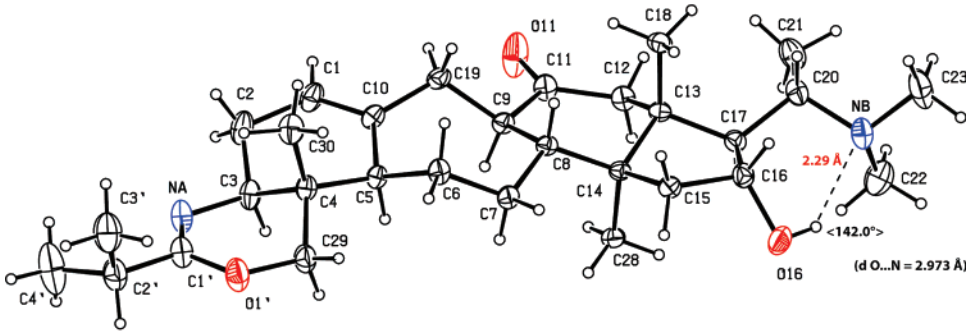

Figure 2. ORTEP representation of the X-ray structure of compound **1** drawn by the Platon program. Dashed line represents the hydrogen bonding.

Scheme 2. Synthesis of Compounds **7a**−**i**, **8a**−**i**, and **9a**−**i**[a]

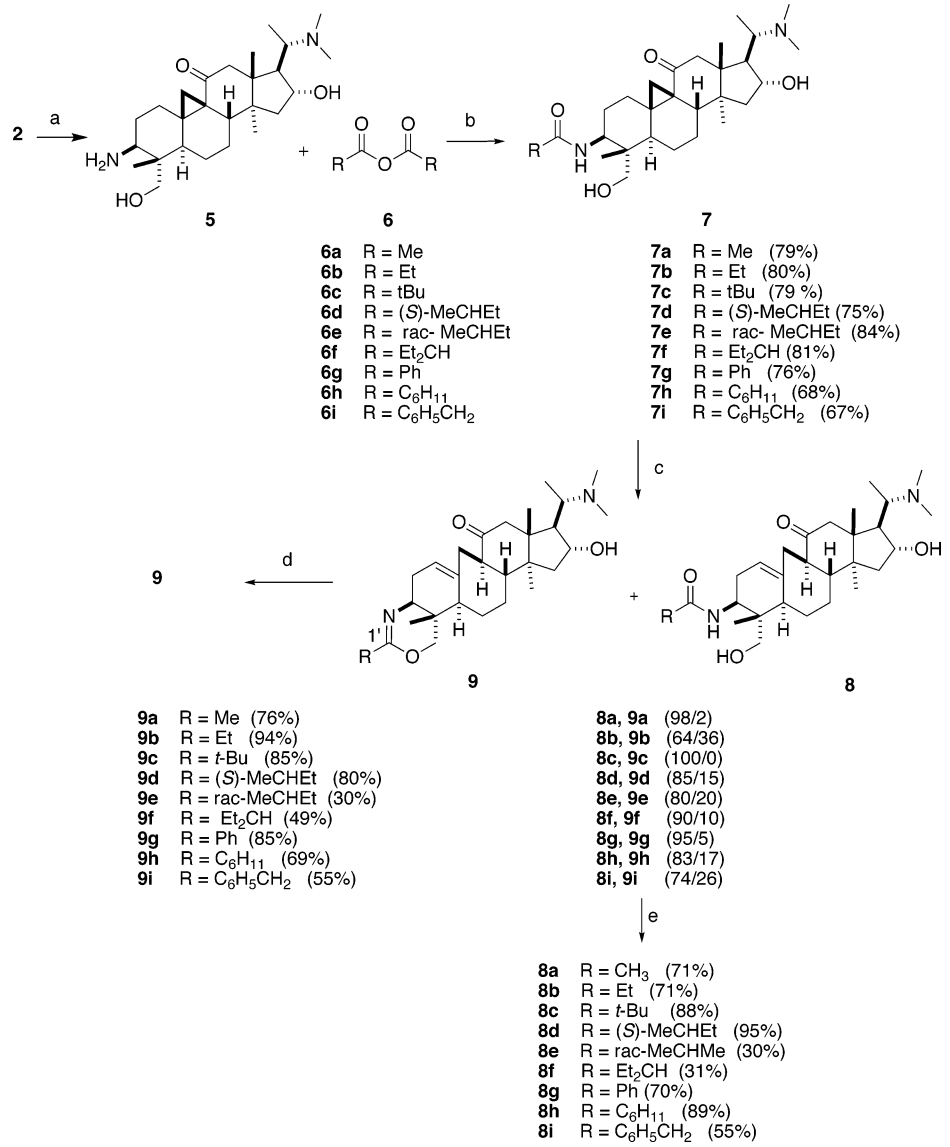

[a] Reagents and conditions: (a) H_2SO_4 (2 N), MeOH, reflux (94%); (b) $(R_1CO)_2O$, **6**, MeOH; (c) 0.03 mmHg, 235 °C to 270 °C; (d) 0.03 mmHg, 235 °C to 270 °C, $Et_4N^+OH^-$; (e) chromatography on alumina.

Scheme 3. Synthesis of Compound **10**[a]

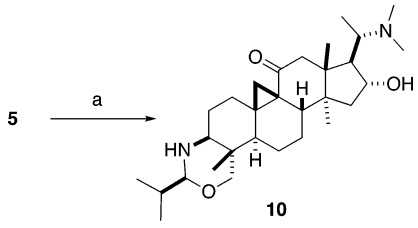

[a] Reagents and conditions: (a) *i*-PrCHO, 1,4-dioxane, 50 °C (30%).

Scheme 4. Synthesis of Compound **12**[a]

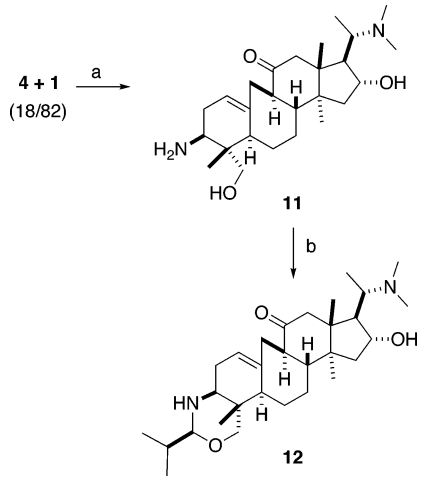

[a] Reagents and conditions: (a) (i) H_2SO_4, MeOH, 2 h, 90 °C; (ii) H_2SO_4, 1 h, 80 °C (60%); (b) *i*-PrCHO, 1,4-dioxane, 50 °C, 12 h (42%).

Results and Discussion

AChE and BuChE Inhibitory Activity. To determine the potential interest of the newly synthesized compounds for the treatment of AD, their AChE inhibitory activity was assayed by the method of Ellman[32] using AChE from *Electrophorus electricus*, *Torpedo californica*, bovine erythrocytes, and human recombinant with tacrine and galanthamine as reference compounds. Moreover, to further study the biological profiles of the novel compounds, their BuChE inhibitory activity on human serum butyrylcholinesterase (hBuChE) was also determined by the same method. Recent studies have shown that, in AD

Scheme 5. Synthesis of Compound **14**[a]

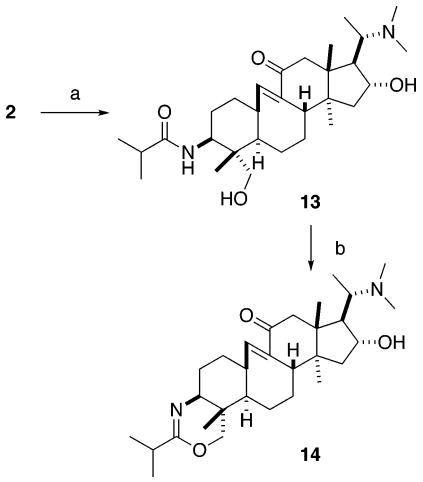

[a] Reagents and conditions: (a) $BF_3{\cdot}Et_2O$, CH_2Cl_2 (86%); (b) $Et_4N^+OH^-$, 300 °C, 0.03 mmHg, 4 h (62%).

Scheme 6. Synthesis of Compounds **15** and **16**[a]

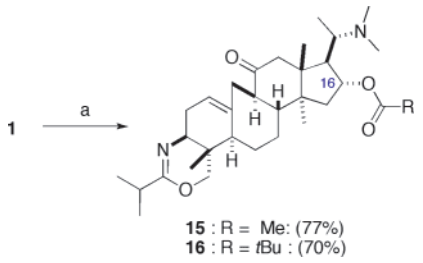

[a] Reagents and conditions: (a) RCOCl, pyridine, rt, 2−3 h.

Scheme 7. Synthesis of Compound **19**[a]

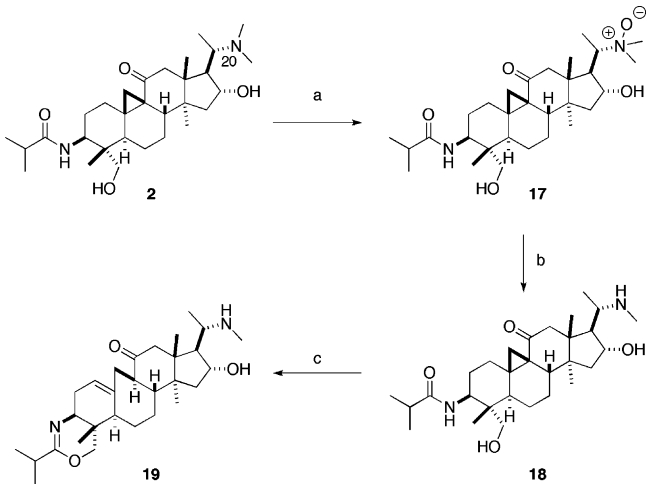

[a] Reagents and conditions: (a) *m*CPBA, CH_2Cl_2, rt, 30 min (79%); (b) (i) $FeSO_4{\cdot}7H_2O$, $FeCl_3{\cdot}6H_2O$, MeOH, rt, 1 h and 30 min; (ii) AcOH/AcONa buffer, CH_2Cl_2 (76%); (c) $Et_4N^+OH^-$, 240 °C, 0.03 mmHg (60%).

patients with severe pathology, BuChE increases while AChE is reduced in specific brain regions;[33] this is not in agreement with a recent study, which shows a decrease of BuChE activity in vivo.[34]

The results are summarized in Tables 1 and 2.

The inhibitory potency depends on numerous factors. Oxazines (**9d**−**h**, 4−32-fold) and pyrimidines (**26a**,**b** and **33**, 13−74-fold) compounds are, in general, more active than their corresponding open precursors (**8d**−**f**, **25a**,**b**, **32**). When the oxazine ring (i.e., **1**) is reduced into oxazinane (i.e., **12**), the inhibitory potency greatly decreases (76-fold). These results suggest that the oxazine and the amidine functions are essential for anticholinesterase activity.

The presence of the cyclopropane ring increases the AChE inhibition potency in the oxazinane (i.e., **10** is 3-fold more active than **12**) and pyrimidine series (**26b** is 2-fold more active than **33**).

A pyrimidine with an open cyclopropane ring (i.e., **33**) is two times less-active than the corresponding oxazine (i.e., **9d**), whereas pyrimidines with a cyclopropane ring (**26a**,**b**) are equipotent or slightly more potent compared to oxazines **1** and **9d**. The influence of the cyclopropane ring on the conformation of the terpene can be seen by the superposition of the two molecules **26a** and **33**; the total curvature of the molecules is not the same, leading to a 3 Å difference at the level of carbon 1′, which could explain the modified activity (Figure 3). Similar conclusions could be observed concerning the influence of the double bond.

Modifying the group at position 1′ of the oxazine and the pyrimidine rings affected the affinity for AChE and BuChE. An order of binding to AChE can be established among the various substituents: $CH_3 < C_2H_5 < CH(CH_3)_2 \leq CH(CH_3)(C_2H_5) >> C(CH_3)_3 > C_6H_{11} >> CH_2{-}Ph > Ph$. The best substituent in this position is (*S*)-MeCHEt (i.e., **9d**, $IC_{50} = 13$ nM). From this list it can be seen that a certain degree of hydrophobicity must be present, while steric hindrance appears as soon as the chain is longer than three linear carbons. It should also be noticed that the presence of a hydrogen on carbon 2′ seems to be necessary, perhaps due to a possible mesomeric form with the vicinal CN double bond.

Transformation of the alcohol function in position 16 into an ester (i.e., **15**, $IC_{50} = 380$ nM; **16**, $IC_{50} = 110$ nM), demethylation of the nitrogen atom in position 20 (i.e., **19**, $IC_{50} = 106$ nM; **1**, $IC_{50} = 31$ nM), and isomerization of the γ,δ-unsaturated ketone (i.e., **1**) into an α,β-unsaturated ketone (i.e., **14**, $IC_{50} = 110$ nM) are all detrimental to the AChE inhibitory activity.

Regarding the BuChE inhibitory activity, the novel compounds reported in this study are weak inhibitors of *h*BuChE (IC_{50} values from 0.37 μM to 7.4 μM; i.e., **9h**, $IC_{50} = 0.37$ μM; **4**, $IC_{50} = 7.4$ μM in the most active compounds, Table 1). So, some of the novel compounds are weak inhibitors of *h*BuChE, but in the range of previously reported steroidal alkaloids.[21−25]

On the basis of the preceding results, steroidal alkaloids **1**, **9a**−**d**, **16**, **19**, **26a**, **26b**, and **33**, which were the most potent inhibitors in *Electrophorus electricus* AChE, were also assayed in *Torpedo californica* AChE, bovine erythrocyte AChE, and human recombinant AChE.

The most potent inhibitors of *Ee*AChE and *Tc*AChE are less active on *b*AChE and *h*AChE. Differences in the primary sequences of cholinesterases from different species could in all likelihood explain the variations in IC_{50} for all these compounds. The primary sequences of *Ee*AChE and *Tc*AChE are very similar but differ from those of *b*AChE and *h*AChE, which are equivalent (84% overall identity). The increased selectivity toward *Ee*AChE and especially *Tc*AChE can be explained by the charge distribution around the peripheral site. For instance, the anionic residue Glu 75 and hydrophilic residue Gln 76 in *Tc*AChE are replaced by the more neutral amino acids Thr and Leu in *h*AChE. At the opening of the gorge, Asp 273 in *Ee*AChE is replaced by Val in *h*AChE and Glu in *Tc*AChE. These modifications could affect the binding of pyrimidines **26a**, **26b**, and **33** because there are more negative charges in *Tc*AChE

Scheme 8. Synthesis of Compounds **26a**,**b**[a]

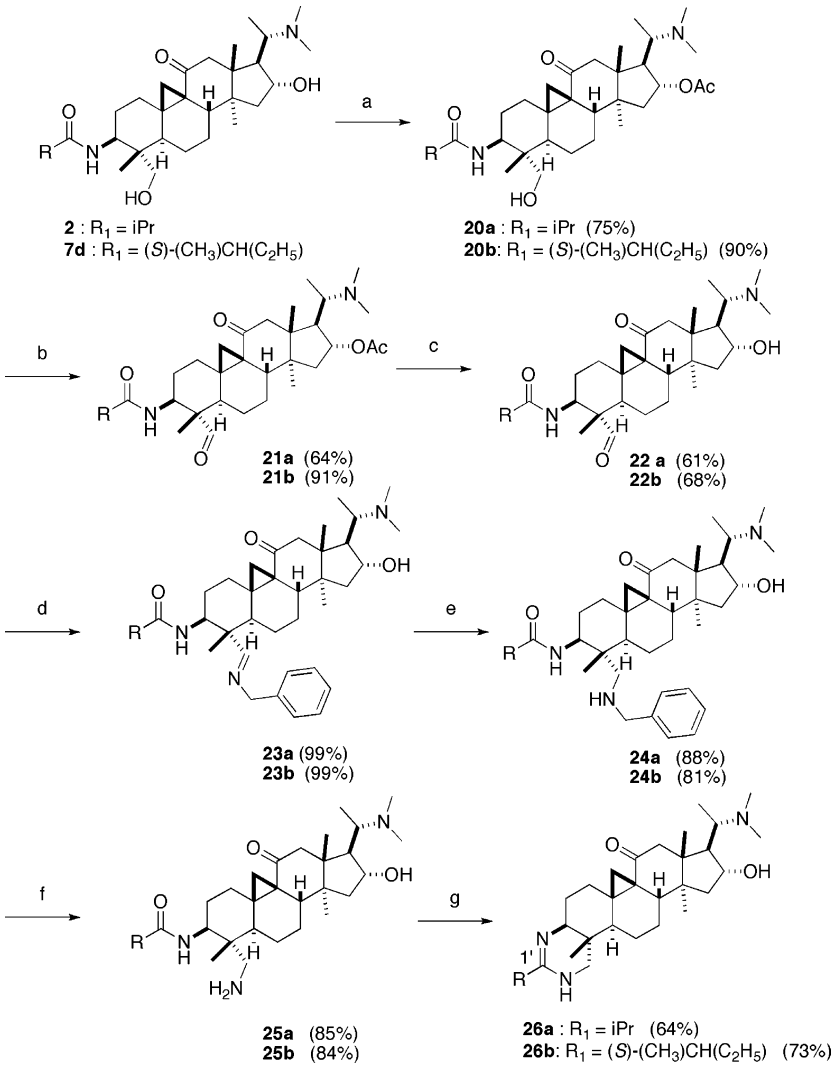

[a] Reagents and conditions: (a) Ac_2O, pyridine, CH_2Cl_2; (b) Dess−Martin periodinane, CH_2Cl_2; (c) $NaHCO_3$, Na_2CO_3, MeOH, H_2O; (d) benzylamine, $MgSO_4$, CH_2Cl_2; (e) $NaBH_3CN$, AcOH, MeOH; (f) $HCOONH_4$, Pd/C 30%, MeOH; (g) Et_3N, *n*-BuOH.

than in *h*AChE at the peripheral site, which increase the favorable interaction of positively charged pyrimidines with the protein.

Within the peripheral site, another example of the variation in charge distribution as a function of the species is given by the two neutral residues Val 277 and Asn 280 in *Tc*AChE, which are replaced by two histidines in *h*AChE. Concerning the gorge of the site, it should be noted that Phe 330 in *Tc*AChE is replaced by a Tyr in *h*AChE and EeAChE. This replacement could thus be the best explanation for a better binding of pyrimidines on TcAChE than on EeAChE in comparison to the binding of oxazine **1**.

Determination of the type inhibition could be interesting, especially by comparison with another inhibitor **34** that we have recently studied (Figure 4).[20b]

From Figure 5, which shows Lineweaver−Burk plots of compounds **26a** and **34** realized under the same conditions, we can see that the two systems are different (mixed type for **26a** and competitive for **34**), and the type of inhibition by **26a** is closer to that of compounds structurally related to those mentioned in previous work.[35] Another example is given by decamethonium, an AChE inhibitor interacting with both sites (see below). Its inhibition type is noncompetitive,[36] for a total length between the two nitrogens identical to that of compounds of type **1**. From these experiments it seems difficult to determine the orientation of the molecules within either the active or the peripheral binding sites. Consequently, molecular modeling was used to bring some insight concerning enzyme−inhibitor interactions.

Molecular Modeling Studies. A molecular modeling study using Discover Biosym was performed to explore the binding of **1** to the enzyme *Tc*AChE (see Experimental Section for details). The crystal structure of the decamethonium−AChE complex[37] was taken as a model because of the similarity of the length between the nitrogen atoms in both compounds and the good superposition of the triterpene skeleton with the decamethonium chain (Figure 6).

The main problem in the study of the interaction of these compounds is determination of the orientation of the molecule in the site, that is to say, situation I (ring D and the dimethyl amino group in the catalytic area) or on the contrary, situation II (ring A and oxazine ring at this location).

It could be observed that the binding of these molecules seems to be very sensitive to the nature of the substituent on the oxazine, which is better taken into account by the catalytic site where steric or ionic constraints are more important (situation II). However, the charge probably resides more on the nitrogen

Scheme 9. Synthesis of Compound **33**[a]

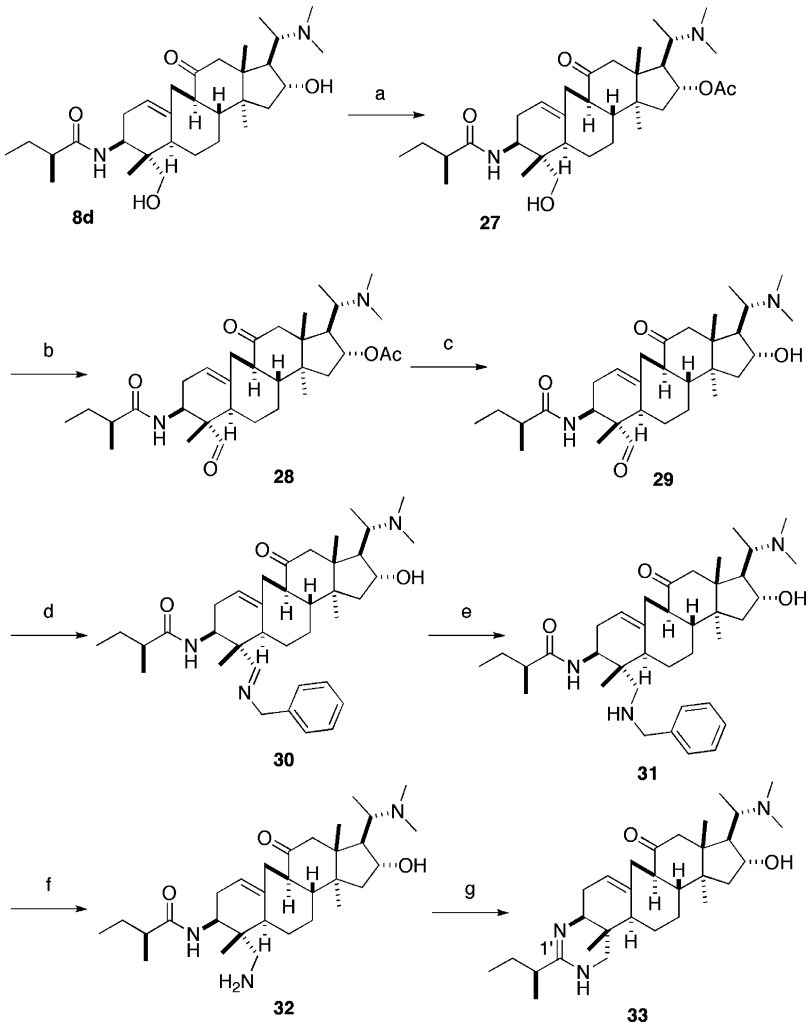

[a] Reagents and conditions: (a) Ac_2O, pyridine, CH_2Cl_2 (90%); (b) Dess−Martin periodinane, CH_2Cl_2 (77%); (c) $NaHCO_3$, Na_2CO_3, MeOH, H_2O (84%); (d) benzylamine, $MgSO_4$, CH_2Cl_2 (99%); (e) $NaBH_3CN$, AcOH, MeOH (73%); (f) $HCOONH_4$, Pd/C 30%, MeOH (36%); (g) Et_3N, *n*-BuOH (49%).

Table 1. Inhibition of *Electrophorus electricus* AChE and human BChE Activities for **1** and its Analogs

	IC_{50} (nM)			IC_{50} (nM)	
cmpd	*Ee*AChE[a]	*h*BuChE[b]	cmpd	*Ee*AChE[a]	*h*BuChE[b]
1	31 ± 4	>1000	**12**	2380 ± 250	>10 000
2	>10 000	>10 000	**14**	110 ± 10	1450 ± 160
4	9380 ± 1200	7407 ± 910	**15**	380 ± 35	N.T.[c]
8d	105 ± 9	>10 000	**16**	110 ± 9	N.T.
8e	120 ± 13	1926 ± 250	**18**	110 ± 11	1440 ± 170
8f	3270 ± 250	>10 000	**19**	106 ± 15	N.T.
9a	680 ± 55	>10 000	**25a**	291 ± 28	N.T.
9b	607 ± 70	>10 000	**25b**	1341 ± 132	N.T.
9c	225 ± 15	>10000	**26a**	18 ± 2	>10 000
9d	13 ± 2	>10 000	**26b**	14 ± 2	N.T.
9e	27 ± 3	>10 000	**30**	780 ± 95	>10 000
9f	102 ± 8	1535 ± 145	**32**	368 ± 40	>10 000
9g	7650 ± 960	>10 000	**33**	28 ± 4	>10 000
9h	400 ± 35	375 ± 35	tacrine	74 ± 8	58 ± 7
9i	4205 ± 410	380 ± 45	galanthamine	360 ± 40	>10 000
10	820 ± 75	>10 000			

[a] *Ee*AChE from *Electrophorus electricus.* [b] BuChE from human serum. [c] Not tested.

atom of the dimethyl amino group and it is known that cations are more stabilized by π-stacking in the catalytic area (situation I; Figure 7).

A previous study of the binding of related molecules to AChE showed an orientation of this type of molecule according to situation II. However, molecules had two protonable nitrogen atoms on ring A and ring D, such that the charge distribution is different from our molecules. The conclusions reached by these experiments thus support those of our study.[38]

To validate the choice of the model (I or II), we decided to compare the binding of different judiciously chosen analogs of **1** and retain the model, which gives the right order of their binding to AChE of *Torpedo californica*, the latter being the enzyme studied in the X-ray studies.

Table 2. Inhibition of Different Sources of AChE by **1** and Selected Analogs

cmpd	IC_{50} (nM)			
	*Ee*AChE[a]	*Tc*AChE[b]	*b*AChE[c]	*h*AChE[d]
1	31	385	756	299
9a	680	2792	6116	5242
9c	225	372	1176	351
9d	13	237	1364	265
16	110	724	1385	839
19	106	485	2226	517
26a	18	2	3277	3108
26b	14	2	6486	4368
33	28	447	7351	3832
tacrine	74	157	446	1030
galanthamine	360			

[a] *Ee*AChE from *Electrophorus electricus*. [b] *Tc*AChE from *Torpedo californica*. [c] *b*AChE from bovine erythrocytes. [d] *h*AChE from *human* recombinant.

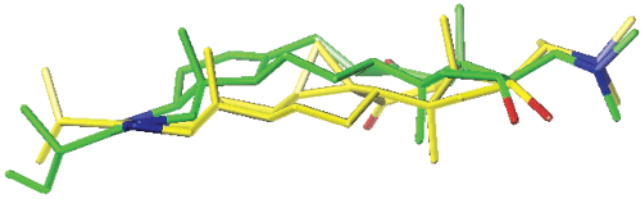

Figure 3. Superposition of the two molecules **26a** (yellow) and **33** (green).

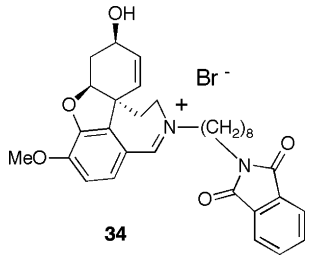

34

Figure 4. Structure of a dual binding site inhibitor in the galanthamine series.

The selected molecules were **1**, **9a**, **9c**, **16**, and **26a**.

The results (see details in Experimental Section) show that for each compound, model I is favored because its energy is slightly lower than the energy of model II (Figure 8). On the other hand, total energy is correlated to activity (IC_{50}) in the case of type II. The correlation between IC_{50} and δE_2_II is qualitative rather than quantitative. The most active compound has the strongest gain in energy, but the IC_{50} differences are not totally accounted for by the energy differences in type I. This could be due to the simplicity of the force-field used in this study. Resorting to more elaborate polarizable molecular mechanics could possibly be envisaged for refinement of the energy balances[39] but is outside the scope of the present work. We also note that the sole entropy effects encompassed in the energy balances δE_2 are those inherent to the continuum solvation energies ΔG_{solv}. The absolute magnitudes of δE_2 are known to be overestimated in the absence of entropy effects that account for the reduction of translational and rotational motions of the ligand upon complex formation.[40] Additional reasons for such overestimations could reside in the above-mentioned simplicity of the force-field as well as to some imbalance in the δE_1 versus δE_{solv} values whose difference (in absolute values) leads to δE_2. Free energy calculations with classical force fields[41] could perhaps provide more realistic estimates of δE_2, but are extremely time-consuming and could also be fraught with uncertainties due inter alia to the lack of polarization effects, which could be very significant in cation-π and stacked complexes.

According to model II, the inflexible steroid **1** enters the aromatic gorge through the six membered A ring and the oxazidine ring. The latter rings are placed at the bottom of the gorge, which might be due to the apparently greater hydrophobicity of these rings in comparison with that of the five-membered D ring (Figure 9). We cannot exclude a different binding mode of the pyrimidine relative to the oxazine analogs. In the pyrimidine series, the nitrogen atoms (calculated pK_a 13) are more basic than the nitrogen atom of the oxazine ring (calculated pK_a 6.5). A protonation of the nitrogen atoms of the pyrimidine ring could thus occur at physiological pH. However, due to the strong structural similarity of this series, this hypothesis does not seem plausible.

Compound **1** is completely buried inside the aromatic gorge. This contributes to the stabilization of the complex since the steroid backbone of **1** is highly hydrophobic due to its aliphatic character. The main hydrophobic interactions between the hydrocarbon skeleton of **1** and the protein were observed with the residues Tyr121, Phe330, Phe331, and Tyr334.

In summary, the type II model seems to be more satisfactory, but further molecular modeling experiments using other molecules will be necessary to allow selection of the correct model. Ideally, an X-ray study of the AChE−inhibitor complex would be required.

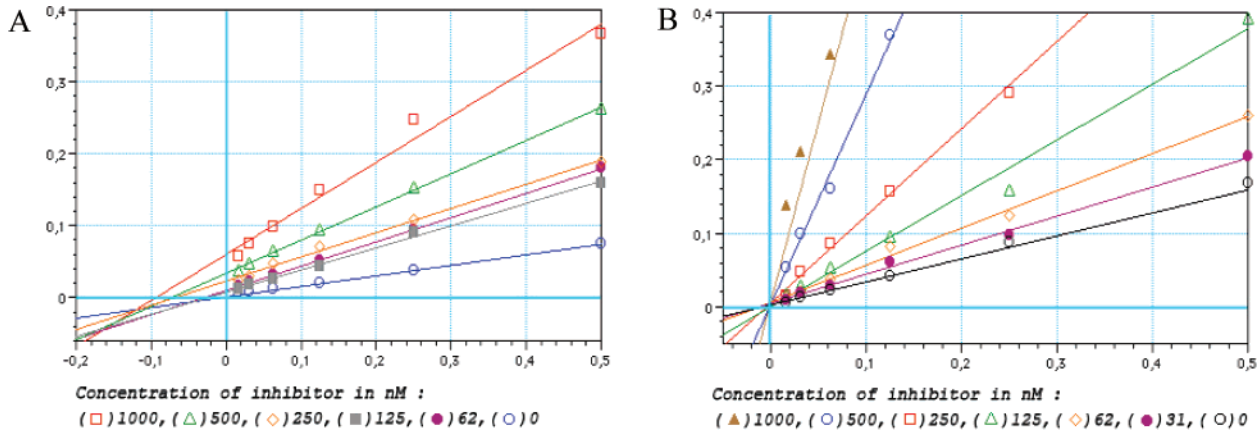

Figure 5. Lineweaver−Burk plots for compounds **26a** (A) and **34** (B). $1/V_{max}$ versus 1/[thioacetylcholine] in the presence of various concentrations of inhibitor (see Experimental Section).

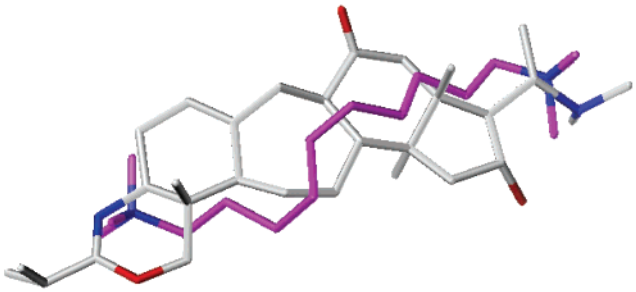

Figure 6. Superposition of decamethonium (magenta) and compound **1**.

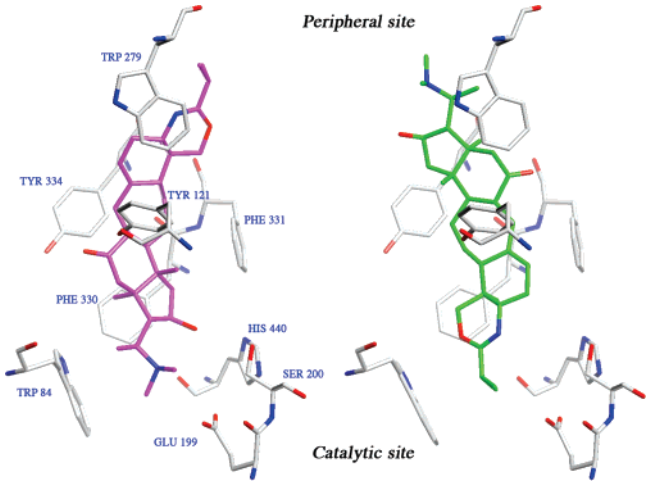

Figure 7. The two models of interaction between **1** and AChE.

Conclusion

We describe a novel series of compounds based on the *N*-3-isobutyrylcycloxobuxidine-F scaffold that are potent and selective inhibitors of AChE. *N*-3-Isobutyrylcycloxobuxidine-F was isolated in large quantities from the leaves of *Buxus balearica* Willd. It is the common precursor of these inhibitors. Beginning from a high-throughput screening, we were able to elaborate a new family of AChE inhibitors, with potencies in the nanomolar range. The oxazine analogs **1** and **9d** are very active on *h*AChE, whereas the pyrimidine analogs **26a** and **26b** are the most potent *Tc*AChE inhibitors. We used these compounds to gain functional and structural insight into the mechanism of inhibition. The tetracyclic triterpene compounds presented herein have a rigid conformation allowing interaction with both peripheral and active sites of AChE, as was shown by molecular modeling studies. The three-dimensional structures of their complexes with AChE will need to be solved by X-ray crystallography.

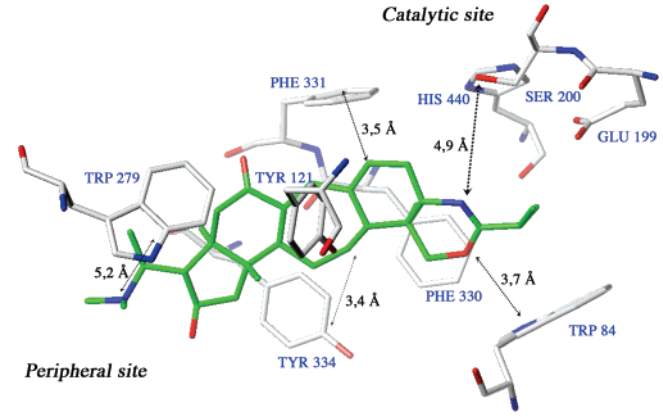

Figure 9. Representation of **1** docked into the binding site of AChE highlighting the protein residues that form the main interactions with the different structural units of the inhibitor.

Experimental Section

Chemistry. All reagents were of commercial quality. All experiments involving water-sensitive compounds were carried out under argon and scrupulously dry conditions, using anhydrous solvents. MeOH was distilled from Mg/I_2, CH_2Cl_2 was distilled from P_2O_5, ethylene glycol was distilled from sodium hydroxide, 1,4-dioxane was distilled from $LiAlH_4$, and NEt_3 and pyridine were distilled from KOH. All separations were carried out under flash chromatographic conditions on Merck silica gel 60 (70−230 mesh) at medium pressure (200 mbar). TLC was performed on Merck silica gel plates ($60F_{254}$) with a fluorescent indicator. NMR spectra were determined on Bruker Avance-300, Bruker AC-400, Bruker AC-500, or Bruker-600 instruments and using tetramethylsilane (TMS) as reference. Chemical shifts are reported in parts per million (ppm) relative to TMS. High-resolution mass spectra (HMRS) were obtained on a MALDI-TOF spectrometer. Infrared (IR) spectra were recorded on a Fourier Perkin-Elmer Spectrum BX FT-IR instruments. Elemental analyses were performed by the microanalysis laboratory of the ICSN, CNRS, Gif-sur-Yvette.

8*H*-Indeno[5′,4′:4,5]cyclohepta[1,2-*f*][3,1]benzoxazin-8-one, 10-[(1*S*)-1-(Dimethylamino)ethyl]-1,4a,5,7,7a,9,9a,10,11,12,12a,12b,13,14,14a,14b-hexadecahydro-11-hydroxy-9a,12a,14b-trimethyl-3-(1-methylethyl)-, (4a*S*,7a*R*,9a*R*,10*S*,11*R*,12a*S*,12b*R*,14a*R*,14b*S*; 1). First procedure was completed in the oven: Compound **2** (100 mg, 0.20 mmol, 1 equiv) is heated at 240 °C under 0.05 mmHg in a rotating distillation oven with four bulbs. A product sublimated in 3 h. The sublimate was composed of a mixture of compound **4** (18%) and the expected dihydro-oxazine **1** (82%). To a solution of the sublimate in 2 mL of dichloromethane was added 25% tetraethylammonium hydroxide (515 mg, 0.87 mmol, 5 equiv) solution in methanol. The solvent was evaporated under reduced pressure. The dark red residue was heated at 240 °C under 0.05 mmHg in a rotating distillation oven with four bulbs during 3 h to give a pale yellow powder of **1** (71.6 mg, 74%) whose spectroscopic characteristics were consistent with described.[30] Second procedure was completed in solution: To a suspension of

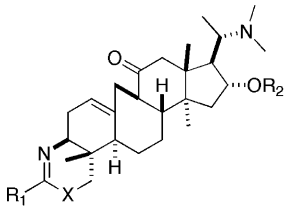

	X	R_1	R_2	δE_{2_I}	δE_{2_II}	IC_{50} *Tc*AChE[a]
1	O	iPr	H	-40.4	-37.2	385
9a	O	Me	H	-41	-24.4	2792
16	O	iPr	COtBu	-45.8	-33.6	724
9c	O	tBu	H	-42.1	-37.2	372
26a	N	iPr	H	-50.3	-40.9	2

[a] *Tc*AChE from *Torpedo californica*

Figure 8. Energy balances (kcal/mol) after single-point Poisson−Boltzmann calculations of continuum solvation energies, and values of the experimentally determined inhibitory potencies IC_{50} (nM) for the molecules selected in our modeling study (see text in the Experimental Section for a definition of the energy values).

compound **2** (50 mg, 0.1 mmol, 1 equiv) in 5 mL of freshly distilled ethylene glycol was added sodium hydroxide (0.8 mg, 0.02 mmol, 0.2 equiv). After heating at 215 °C during 6 h, the mixture was then made basic with 60 mL of a 10% ammonia solution (pH = 10) and extracted with dichloromethane (3 × 40 mL). The organic layer was dried over Na_2SO_4 and filtered, and the solvent was evaporated to give a pale yellow powder of **1** (40 mg, 83%) whose spectroscopic characteristics were consistent with those described.[30] Mp 281.5 °C; $[\alpha]^{25}_D = +71$ (*c* 0.8, $CHCl_3$); IR ($CHCl_3$) υ_{max}(cm^{-1}) 3467, 2966, 1694, 1668, 1466, 1376, 1148, 1037; ^{1}H NMR (600 MHz, $CDCl_3$) δ 0.66 (3H, s, H-18), 0.71 (3H, s, H-30), 0.84 (3H, d, J = 6.6 Hz, H-21), 1.08, 1.09 (6H, 2d, J = 6.9 Hz, H-3′, H-4′), 1.20 (3H, s, H-28), 1.28 (1H, m, H-6β), 1.30 (1H, m, H-7α), 1.47 (1H, dd, J = 2.5, 13.8 Hz, H-15α), 1.59 (1H, dd, J = 7.5, 13.4 Hz, H-6α), 1.63 (1H, ddd, J = 3.7, 10.2, 10.9 Hz, H-8β), 1.74 (1H, m, H-2β), 1.83 (1H, bd, J = 8.3 Hz, H-5α), 1.89 (1H, m, H-7β), 1.89 (1H, dd, J = 9.0, 10.2 Hz, H-9α), 1.96 (1H, m, H-15β), 1.96 (1H, m, H-17α), 2.03 (1H, m, H-19β), 2.20 (6H, bs, NB-*CH*$_3$), 2.31 (1H, d, J = 15.8 Hz, H-12β), 2.31 (1H, m, H-2α), 2.37 (1H, dq, J = 6.9 Hz, H-2′), 2.52 (1H, bd, J = 15.8 Hz, H-12α), 2.57 (1H, dq, J = 6.6, 11.2 Hz, H-20), 3.20 (1H, dd, J = 6.0, 11.7 Hz, H-3α), 3.31 (1H, d, J = 15.5 Hz, H-19α), 3.73 (1H, d, J = 10.2 Hz, H-29α), 4.04 (1H, d, J = 10.2 Hz, H-29β), 4.05 (1H, ddd, J = 2.5, 6.9, 9.7 Hz, H-16β), 5.56 (1H, m, H-1); ^{13}C NMR (125 MHz, $CDCl_3$) δ 9.59 (CH_3, C-30), 9.94 (CH_3, C-21), 17.75 (CH_3, C-18), 18.77 (CH_3, C-28), 19.73, 19.80 (CH_3, C-3′, C-4′), 24.61 (CH_2, C-6), 30.75 (CH_2, C-2), 33.16 (C, C-4), 33.47 (CH_2, C-7), 34.27 (CH, C-2′), 37.27 (CH_2, C-19), 42.44 (CH_2, C-15), 46.14 (C, C-14), 46.97 (C, C-13), 49.44 (CH, C-5), 49.67 (CH, C-8), 49.98 (CH_2, C-12), 50.23 (CH, C-9), 55.46 (CH, C-17), 55.60 (CH, C-3), 61.99 (CH, C-20), 74.72 (CH_2, C-29), 78.27 (CH, C-16), 121.81 (CH, C-1), 137.10 (C, C-10), 162.57 (C, C-1′), 211.55 (C, C-11); ES-MS *m*/*z* 485.3 $[M + H]^+$ (95), 486.3 (100), 487.4 (50), 503.4 (2); HRES-MS *m*/*z* calcd for $C_{30}H_{49}N_2O_3$, 485.3743; found, 485.3721; Anal. Calcd for $C_{30}H_{48}N_2O_3$: C, 74.34%; H, 9.98%; N, 5.78%; O, 9.90%. Found: C, 74.13%; H, 9.91%; N, 5.67%; O, 9.97%.

***N*-3-*iso*-Butyrylcycloxobuxidine-F (2) or *N*-[(3β,4α,9β,16α,20*S*)-20-(Dimethylamino)-16-hydroxy-4-(hydroxymethyl)-4,14-Dimethyl-11-oxo-9,19-cyclopregnan-3-yl]-2-methylpropanamide (2). First Part: Extraction Procedure for Total Alkaloids of *Buxus balearica* Willd.** Dried and pulverized leaves (1.5 kg) from *Balearica buxus* Willd were alkalized with 600 mL of a 30% ammonia solution. A first extraction was achieved after stirring with 10 L of solvents (CH_2Cl_2−EtOH 9:1) at room temperature overnight. After filtration, five successive soakings were carried out with 10 L of solvents (CH_2Cl_2−EtOH 9:1), while stirring at room temperature during 3 h between each filtration.

Collected organic layers were evaporated under reduced pressure to give a crude and dark green extract (240 g). This crude product was washed successively with 7 L of dichloromethane and washed 10 times with 1 L of hydrochloric acid. The aqueous layers were made basic with a 10% ammonia solution (pH = 10), then extracted with dichloromethane (6 × 2 L). The combined organic extracts were evaporated under reduced pressure to give a brown powder (105 g, 7%).

This process was also carried out with 11 kg of *Buxus Balearica* Willd leaves.

Second Part: Extraction of *N*-3-Isobutyrylcycloxobuxidine-F. Procedure for the Preparation of Solutions: A total of 4 L of a 1.0 M AcOH/AcONa buffer solution at pH = 5 were prepared by dissolving glacial acetic acid (17.136 g, 0.2348 mol) and sodium acetate (99.296 g, 0.7151 mol) 1 L of water.

The alkaloids were dissolved four times in the buffer solution at pH = 5.

The solution of total alkaloids (27.3 g) in 500 mL of dichloromethane was washed with 4 × 1 L of the buffer solution at pH = 5. This organic layer was washed successively with 1 L of a 10% ammonia solution, with 1 L of water and 1 L of brine, then dried over Na_2SO_4 and filtered, and the solvent was evaporated to give a residue (1.74 g).

Table 3. Weight of Alkaloid in Function of the pH Extraction

	weight (g)
residue	1.74
pH	
5	4.71
5.8	3.19
6.5	1.80
7.3	4.06
8.2	6.70
9.1	3.25
	total: 25.4 g and a loss of about 1.9 g

The pH of each aqueous layer containing the total alkaloids dissolved in the buffer solution was increased by one pH unit with a 10% ammonia solution. The aqueous layers were washed successively with 8 × 500 mL of dichloromethane until exhaustion of alkaloids in the aqueous layer. The combined organic extracts were washed successively with 1 L of a 10% ammonia solution, with 1 L of water and 1 L of brine, then dried over Na_2SO_4 and filtered, and the solvent was evaporated to give *N*-3-*iso*butyryl-cycloxobuxidine-F **2** (3.19 g, 0.8%) at pH = 5.8. This leads to the weight balance shown in Table 3.

This process was also carried out with 11 kg of *Balearica buxus* Willd leaves. Trituration in acetone gave *N*-3-*iso*-butyrylcycloxo-buxidine-F **2** (100 g, 0.9%), whose spectroscopic characteristics are identical to those described.[30] Mp 257 °C; $[\alpha]^{25}_D = +69$ (*c* 1.01, $CHCl_3$); IR ($CHCl_3$) υ_{max} (cm^{-1}) 3434, 1690, 1654, 1513, 1096; ^{1}H NMR (600 MHz, $CDCl_3$) δ 0.53 (3H, s, H-30), 0.80 (3H, s, H-18), 0.83 (3H, d, J = 6.6 Hz, H-21), 0.85 (1H, dddd, J = 3.6, 11.7, 12.6, 14.5 Hz, H-6β), 1.00 (1H, d, J = 3.8 Hz, H-19β), 1.13, 1.15 (6H, 2d, J = 6.8 Hz, H-3′, H-4′), 1.18 (3H, s, H-28), 1.25 (1H, ddd, J = 4.2, 13.0, 13.5 Hz, H-1α), 1.40 (1H, m, J = 4.0, 10.9, 12.6, 14.5 Hz, H-7α), 1.46 (1H, dd, J = 3.0, 14.0 Hz, H-15α), 1.49 (1H, ddd, J = 3.6, 7.5, 14.5 Hz, H-7β), 1.52 (1H, d, J = 3.8 Hz, H-19α), 1.55 (1H, ddd, J = 4.0, 12.7, 13.0 Hz, H-2β), 1.65 (1H, ddd, J = 3.6, 4.2, 4.2 Hz, H-2α), 1.67 (1H, ddd, J = 3.6, 4.0, 14.5 Hz, H-6α), 1.94 (1H, dd, J = 7.3, 10.8 Hz, H-17α), 1.98 (1H, dd, J = 7.5, 10.9 Hz, H-8β), 1.98 (1H, dd, J = 9.5, 14.0 Hz, H-15β), 2.02 (1H, dd, J = 3.6, 11.7 Hz, H-5α), 2.20 (6H, bs, NB−C*H*$_3$), 2.26 (1H, d, J = 17.1 Hz, H-12β), 2.36 (1H, dq, J = 6.8 Hz, H-2′), 2.38 (1H, ddd, J = 3.6, 4.0, 13.5 Hz, H-1β), 2.48 (1H, d, J = 17.1 Hz, H-12α), 2.58 (1H, dq, J = 6.6, 10.8 Hz, H-20), 2.92 (1H, dd, J = 3.2, 12.5 Hz, H-29a), 3.30 (1H, dd, J = 10.4, 12.5 Hz, H-29b), 3.94 (1H, ddd, J = 4.2, 9.0, 12.7 Hz, H-3α), 4.05 (1H, ddd, J = 3.0, 7.3, 9.5 Hz, H-16β), 4.37 (1H, dd, J = 3.2, 10.4 Hz, O*H*), 5.47 (1H, d, J = 9.0 Hz, NA*H*); ^{13}C NMR (125 MHz, $CDCl_3$) δ 9.87 (CH_3, C-21), 11.15 (CH_3, C-30), 17.79 (CH_3, C-18), 18.36 (CH_2, C-6), 19.38, 20.09 (CH_3, C-3′, C-4′), 20.77 (CH_3, C-28), 24.26 (CH_2, C-7), 27.49 (CH_2, C-2), 27.65 (CH_2, C-1), 30.48 (CH_2, C-19), 34.41 (C, C-9), 35.68 (CH, C-2′), 37.72 (C, C-10), 41.12 (CH, C-5), 41.37 (CH, C-8), 42.76 (CH_2, C-15), 44.45 (C, C-13), 44.50 (C, C-4), 47.09 (C, C-14), 50.64 (CH, C-3), 51.45 (CH_2, C-12), 55.79 (CH, C-17), 61.98 (CH, C-20), 64.11 (CH_2, C-29), 78.27 (CH, C-16), 178.45 (C, C-1′), 211.47 (C, C11); ES-MS *m*/*z* 503.4 $[M + H]^+$ (100), 504.4 (10); HRES-MS *m*/*z* calcd for $C_{30}H_{51}N_2O_4$, 503.3849; found, 503.3852; Anal. Calcd for $C_{30}H_{50}N_2O_4$: C, 71.67%; H, 10.02%; N, 5.57%; O, 12.73%. Found: C, 71.51%; H, 10.14%; N, 5.34%; O, 12.87%.

***N*-[(2*R*,3*S*,3a*R*,5a*R*,9*S*,10*S*,12a*R*,12b*S*)-3-[1-(Dimethylamino)-ethyl]-2-hydroxy-10-(hydroxymethyl)-3a,10,12b-trimethyl-5-oxo-1,2,3,3a,4,5,5a,6,8,9,10,10a,11,12,12a,12b-hexadecahydrobenzo-[4,5]cyclohepta[1,2-*e*]inden-9-yl]-2-methylpropanamide (4).** First procedure in solution: A suspension of compound **2** (250 mg, 0.49 mmol, 1 equiv) in 20 mL of freshly distilled ethylene glycol on sodium hydroxide pellets (concentration about 12 g/L) was stirred for 6 h at 160 °C under inert atmosphere. The mixture was then made basic with 50 mL of a 10% ammonia solution (pH = 10) and extracted with dichloromethane (3 × 40 mL). The organic layer was washed with brine (30 mL), dried over Na_2SO_4, and filtered, and the solvent was evaporated. The crude product was purified

by column chromatography on alumina with dichloromethane−methanol (98:2) as eluent followed by trituration in acetone to afford a colorless powder of **4** (105 mg, 42%), whose spectroscopic characteristics are identical to those described.[30] Second procedure in the oven: Compound **2** (100 mg, 0.20 mmol, 1 equiv) was heated at 240 °C under 0.05 mmHg in a rotating distillation oven with four bulbs. A product sublimated in 3 h. The sublimate was composed of a mixture of the expected product **4** (18%) and dihydrooxazine **1** (82%). The sublimate was purified by column chromatography on alumina with dichloromethane−methanol (98:2) as eluent followed by trituration in acetone to afford a colorless powder of **4** (91 mg, 91%), whose spectroscopic characteristics were consistent and identical to those described.[30] Mp 242 °C; $[\alpha]^{25}_D = -46$ (*c* 1.0, $CHCl_3$); IR ($CHCl_3$) υ_{max} (cm^{-1}) 3433, 1693, 1652, 1513, 1462, 1380, 1097, 1043, 1015; ^1H NMR (300 MHz, $CDCl_3$) δ 0.47 (3H, s, H-30), 0.69 (3H, s, H-18), 0.87 (3H, d, $J = 6.2$ Hz, H-21), 1.19 (6H, 2d, $J = 7.0$ Hz, H-3′, H-4′), 1.27 (3H, s, H-28), 1.29 (1H, m, H-6β), 1.50 (1H, dd, $J = 2.3$, 13.8 Hz, H-15α), 1.58 (1H, bd, $J = 11.7$ Hz, H-7α), 1.64 (1H, m, H-8β), 1.83 (1H, m, H-6α), 1.88 (1H, m, H-7β), 1.92 (1H, m, H-2β), 1.99 (1H, m, H-15β), 2.02 (1H, dd, $J = 7.0$, 11.0, H-17α), 2.03 (1H, m, H-9α), 2.08 (1H, m, H-19β), 2.24 (6H, bs, NB-*CH*$_3$), 2.28 (1H, m, H-2α), 2.34 (1H, d, $J = 16.0$ Hz, H-12β), 2.42 (1H, m, $J = 7.0$ Hz, H-2′), 2.44 (1H, m, H-19β), 2.58 (1H, bd, $J = 16.0$ Hz, H-12α), 2.59 (1H, m, H-20), 2.60 (1H, m, H-5α), 3.10 (1H, dd, $J = 4.3$, 11.0 Hz, H-29a), 3.35 (1H, d, $J = 13.9$ Hz, H-19α), 3.38 (1H, m, H-29b), 4.08 (1H, m, H-3α), 4.09 (1H, m, $J = 6.6$ Hz, H-16β), 4.57 (1H, dd, $J = 4.3$, 10.6 Hz, O*H*), 5.32 (1H, d, $J = 8.9$ Hz, NA*H*), 5.48 (1H, m, H-1); ^{13}C NMR (75.5 MHz, $CDCl_3$) δ 9.9 (CH_3, C-21), 10.0 (CH_3, C-30), 17.8 (CH_3, C-18), 19.0, 19.5 (CH_3, C-3′, C-4′), 20.1 (CH_3, C-28), 25.0 (CH_2, C-6), 30.0 (CH_2, C-2), 33.5 (CH_2, C-7), 35.9 (CH, C-2′), 37.6 (CH_2, C-19), 42.1 (C, C-4), 42.4 (CH_2, C-15), 43.4 (CH, C-5), 46.2 (C, C-14), 47.1 (C, C-13), 47.7 (CH, C-3), 49.9 (CH, C-8), 50.0 (CH_2, C-12), 50.1 (CH, C-9), 55.3 (CH, C-17), 62.0 (CH, C-20), 63.8 (CH_2, C-29), 78.4 (CH, C-16), 117.9 (CH, C-1), 140.0 (C, C-10), 178.9 (C, C-1′), 212.1 (C, C-11); ES-MS *m*/*z* 503.3 $[M + H]^+$ (100), 504.3 (90); HRES-MS *m*/*z* calcd for $C_{30}H_{51}N_2O_4$, 503.3849; found, 503.3852. Anal. ($C_{30}H_{50}N_2O_4 \cdot 0.5H_2O$) C, H, N.

***N*-3-Benzoylcycloxobuxidine-F (3) or *N*-[(3β,4α,5α,9β,16α,20S)-20-(Dimethylamino)-16-hydroxy-4-(hydroxymethyl)-4,14-dimethyl-11-oxo-9,19-cyclopregnan-3-yl]benzamide (7g).** To a solution of cycloxobuxidine-F **5** (166 mg, 0.38 mmol, 1 equiv) in 10 mL of methanol was added benzoic anhydride (95 mg, 0.46 mmol, 1.1 equiv). After stirring for 4 h at room temperature, the mixture was neutralized with a few drops of a 10% sodium bicarbonate solution (pH = 8), then made basic with 50 mL of a 10% ammonia solution (pH = 10), and extracted with dichloromethane (3 × 40 mL). The organic layer was washed with brine (30 mL), dried over Na_2SO_4, and filtered, and the solvent was evaporated. The crude product was purified by column chromatography on alumina with dichloromethane−methanol (98:2) as eluent followed by trituration in acetone to afford a colorless powder of **7g** (156 mg, 76%), whose spectroscopic characteristics are identical to those described.[30] Mp 277 °C; $[\alpha]^{25}_D = +52$ (*c* 1.00, $CHCl_3$); IR ($CHCl_3$) υ_{max} (cm^{-1}) 3438, 1645, 1628, 1518, 1487, 1384, 1040; ^1H NMR (300 MHz, $CDCl_3$) δ 0.65 (3H, s, H-30), 0.85 (3H, s, H-18), 0.88 (3H, d, $J = 6.6$ Hz, H-21), 0.92 (1H, m, H-6β), 1.03 (1H, d, $J = 3.8$ Hz, H-19α), 1.24 (3H, s, H-28), 1.34 (1H, m, H-1α), 1.42 (1H, m, H-7α), 1.52 (1H, dd, $J = 2.6$, 14.1 Hz, H-15α), 1.55 (1H, m, H-7β), 1.60 (1H, d, $J = 3.8$ Hz, H-19β), 1.70 (1H, m, H-2β), 1.75 (2H, m, H-6α, H-2α), 1.99 (1H, m, H-17α), 2.03 (1H, m, H-15β), 2.07 (1H, m, H-8β), 2.14 (1H, dd, $J = 3.3$, 12.1 Hz, H-5α), 2.26 (6H, bs, NB-*CH*$_3$), 2.32 (1H, d, $J = 17.2$ Hz, H-12β), 2.47 (1H, ddd, $J = 3.0$, 3.3, 13.6 Hz, H-1β), 2.54 (1H, d, $J = 17.2$ Hz, H-12α), 2.63 (1H, dq, $J = 6.6$, 10.8 Hz, H-20), 3.12 (1H, dd, $J = 3.4$, 12.7 Hz, H-29a), 3.40 (1H, dd, $J = 10.4$, 12.7 Hz, H-29b), 4.12 (1H, ddd, $J = 3.0$, 7.3, 10.0 Hz, H-16β), 4.24 (1H, ddd, $J = 4.3$, 8.9, 12.5 Hz, H-3α), 4.44 (1H, dd, $J = 3.4$, 10.4 Hz, O*H*), 6.05 (1H, d, $J = 8.9$ Hz, NA*H*), 7.48, 7.76 (5H, m, HAr = 3′,4′,5′,6′,7′); ^{13}C NMR (75.5 MHz, $CDCl_3$) δ 10.0 (CH_3, C-21), 11.4 (CH_3, C-30), 17.9 (CH_3, C-18), 18.4 (CH_2, C-6), 20.9 (CH_3, C-28), 24.4 (CH_2, C-7), 27.7 (CH_2, C-1), 27.7 (CH_2, C-2), 30.6 (CH_2, C-19), 34.5 (C, C-9), 37.8 (C, C-10), 41.3 (CH, C-5), 41.4 (CH, C-8), 42.8 (CH_2, C-15), 44.5 (C, C-4), 44.9 (C, C-13), 47.2 (C, C-14), 51.5 (CH, C-3), 51.7 (CH_2, C-12), 55.8 (CH, C-17), 62.1 (CH, C-20), 64.3 (CH_2, C-29), 78.3 (CH, C-16), 127.0, 128.8 (CH, C−Ar = 3′,4′,6′,7′), 131.9 (C, C-5′), 133.9 (C, C-2′), 168.8 (C, C-1′), 211.6 (C, C-11); ES-MS *m*/*z* 537.4 $[M + H]^+$ (100), 538.4 (15); HRES-MS *m*/*z* calcd for $C_{33}H_{49}N_2O_4$, 537.3692; found, 537.3679. Anal. ($C_{33}H_{48}N_2O_4 \cdot 0.5H_2O$) C, H, N, O.

***N*-[(2*R*,3*S*,3a*R*,5a*R*,9*S*,10*S*,10a*R*,12a*R*,12b*S*)-3-[(1*S*)-1-(Dimethylamino)ethyl]-1,2,3,3a,4,5,5a,6,8,9,10,10a,11,12,12a,12b-hexadecahydro-2-hydroxy-10-(hydroxymethyl)-3a,10,12b-trimethyl-5-oxobenzo[4,5]cyclohept[1,2-*e*]inden-9-yl]acetamide (8a).** Compound **7a** (221 mg, 0.46 mmol, 1 equiv) was heated at 240 °C under 0.03 mmHg in a rotating distillation oven with four bulbs. A product sublimated in 3 h. The sublimate was composed of a mixture of the expected product **8a** (98%) and dihydrooxazine **9a** (2%). The sublimate was purified by column chromatography on alumina with dichloromethane−methanol (99.7:0.3) as eluent followed by trituration in acetone to afford a colorless powder of **8a** (79.4 mg, 88%). Mp 253 °C; IR ($CHCl_3$) υ_{max} (cm^{-1}) 3435, 2928, 1694, 1654, 1516, 1462, 1375, 1095, 1043; ^1H NMR (300 MHz, $CDCl_3$) δ 0.46 (3H, s, H-30), 0.67 (3H, s, H-18), 0.85 (3H, d, $J = 6.2$ Hz, H-21), 1.27 (3H, s, H-28), 1.28 (1H, m, H-6β), 1.43 (1H, dd, $J = 2.3$, 13.9 Hz, H-15α), 1.58 (1H, bd, $J = 11.9$ Hz, H-7α), 1.57 (1H, m, H-8β), 1.76 (1H, m, H-6α), 1.81 (1H, m, H-7β), 1.88 (1H, m, H-2β), 1.89 (1H, m, H-15β), 1.92 (1H, m, H-9α), 2.02 (1H, m, H-17α), 2.04 (1H, s, H-2′), 2.11 (1H, m, H-19β), 2.22 (6H, bs, NB-*CH*$_3$), 2.28 (1H, m, H-2α), 2.32 (1H, d, $J = 15.8$ Hz, H-12β), 2.56 (1H, bd, $J = 15.8$ Hz, H-12α), 2.58 (1H, m, H-5α), 2.59 (1H, m, H-20), 3.17 (1H, dd, $J = 4.5$, 12.7 Hz, H-29a), 3.33 (1H, d, $J = 14.5$ Hz, H-19α), 3.40 (1H, m, H-29b), 4.04 (1H, m, H-3α), 4.07 (1H, m, H-16β), 4.53 (1H, dd, $J = 4.5$, 11.0 Hz, O*H*), 5.46 (1H, bs, H-1), 5.50 (1H, d, $J = 8.9$ Hz, NA*H*); ^{13}C NMR (75.5 MHz, $CDCl_3$) δ 9.9 (CH_3, C-21), 10.0 (CH_3, C-30), 17.8 (CH_3, C-18), 18.9 (CH_3, C-28), 23.3 (CH, C-2′), 24.9 (CH_2, C-6), 29.9 (CH, C-2), 33.5 (CH_2, C-7), 37.5 (CH_2, C-19), 42.0 (C, C-4), 42.4 (CH_2, C-15), 43.4 (CH, C-5), 46.2 (C, C-14), 47.0 (C, C-13), 48.4 (CH, C-3), 49.9 (CH, C-8), 50.0 (CH_2, C-12), 50.1 (CH, C-9), 55.3 (CH, C-17), 62.0 (CH, C-20), 63.8 (CH_2, C-29), 78.4 (CH, C-16), 117.9 (CH, C-1), 140.0 (C, C-10), 172.0 (C, C-1′), 212.1 (C, C-11); ES-MS *m*/*z* 475.3 $[M+H]^+$ (100), 476.3 (60); HRES-MS *m*/*z* calcd for $C_{28}H_{47}N_2O_4$, 475.3536; found, 475.3548.

(4a*S*,7a*R*,9a*R*,10*S*,11*R*,12a*S*,12b*R*,14b*S*)-10-[1-(Dimethylamino)ethyl]-11-hydroxy-3,9a,12a,14b-tetramethyl-1,4a,5,7,7a,9,9a,10,11,12,12a,12b,13,14,14a,14b-hexadecahydro-8*H*-indeno-[5′¢,4′¢:4′,5′]cyclohepta[1′,2′:3,4]benzo[1,2-*d*][1,3]oxazin-8-one (9a). To a solution of compound **7a** (171 mg, 0.36 mmol, 1 equiv) in 2 mL of dichloromethane was added 25% tetraethylammonium hydroxide (1059 mg, 1.8 mmol, 5 equiv) solution in methanol. The solvent was evaporated under reduced pressure. The dark red residue was heated at 240 °C under 0.03 mmHg in a rotating distillation oven with four bulbs. A product sublimated in 3 h. This crude product was crystallized in acetone to afford a pale yellow powder of **9a** (125 mg, 76%): mp 284 °C; $[\alpha]^{23}_D = +123$ (*c* 0.25, $CHCl_3$); IR ($CHCl_3$) υ_{max} (cm^{-1}) 3331, 2971, 1694, 1672, 1462, 1383, 1039; ^1H NMR (300 MHz, $CDCl_3$) δ 0.70 (3H, s, H-18), 0.79 (3H, s, H-30), 0.87 (3H, d, $J = 6.6$ Hz, H-21), 1.24 (3H, s, H-28), 1.29 (1H, m, H-6β), 1.33 (1H, m, H-7α), 1.50 (1H, dd, $J = 2.3$, 13.7 Hz, H-15α), 1.63 (1H, m, H-6α), 1.66 (1H, m, H-8β), 1.74 (1H, m, H-2β), 1.83 (1H, m, H-5α), 1.89 (1H, m, H-7β), 1.92 (3H, s, H-2′), 1.96 (1H, m, H-9α), 2.02 (1H, m, H-15β), 2.03 (1H, m, H-17α), 2.09 (1H, m, H-19β), 2.24 (6H, bs, NB-*CH*$_3$), 2.34 (1H, d, $J = 16.0$ Hz, H-12β), 2.30 (1H, m, H-2α), 2.56 (1H, bd, $J = 16.0$ Hz, H-12α), 2.60 (1H, dd, $J = 6.6$, 11.0 Hz, H-20), 3.25 (1H, dd, $J = 6.0$, 12.0 Hz, H-3α), 3.34 (1H, d, $J = 15.4$ Hz, H-19α), 3.79 (1H, d, $J = 10.2$ Hz, H-29α), 4.06 (1H, d, $J = 10.2$ Hz, H-29β), 4.09 (1H, m, H-16β), 5.60 (1H, m, H-1); ^{13}C NMR (75.5 MHz, $CDCl_3$) δ 9.9 (CH_3, C-30), 10.0 (CH_3, C-21), 17.8 (CH_3, C-18), 18.8 (CH_3, C-28), 21.0 (CH_3, C-2′), 24.6 (CH_2, C-6), 30.6

Table 4. Energy Balances (kcal/mol) after Single-Point Poisson−Boltzmann Calculations of Continuum Solvation Energies, and Values of the Experimentally Determined Inhibitory Potencies IC_{50} (nM)[a]

cmpd	type[b]	E_{tot}	E_{lig}	δE_1	$E_{solvtot}$	$E_{solvlig}$	δE_{solv}	δE_2	IC_{50} (nM)
1	I	−10 500.0	1.4	−120.8	−1529.2	−17.3	80.4	−40.4	385
1	II	−10 495.0	1.4	−115.8	−1531.0	−17.3	78.6	−37.2	385
9a	I	−10 502.0	0.4	−121.8	−1529.4	−17.5	80.0	−41.0	2790
9a	II	−10 491.0	0.4	−110.8	−1523.3	−17.5	86.3	−24.4	2790
15	I	−10 483	24.6	−127.	−1527.5	−16.6	81.2	−45.8	525
15	II	−10 460	24.6	−104.	−1538.3	−16.6	70.4	−33.6	525
9c	I	−10 502	4	−125.4	−1526.3	−17.8	83.3	−42.1	372
9c	II	−10 492	4	−115.4	−1531.4	−17.8	78.3	−37.2	372
26a	I	−10 566.3	1.6	−184.6	−1498.1	−40.6	134.3	−50.3	2
26a	II	−10 568.6	1.6	−187.	−1486.3	−40.6	146.1	−40.9	2

[a] Given in nanomoles (see text for definition of the energy values). [b] Type I: oxazine ring at peripheral site; type II: oxazine ring at catalytic site.

(CH_2, C-2), 32.9 (C, C-4), 33.5 (CH_2, C-7), 37.2 (CH_2, C-19), 42.4 (CH_2, C-15), 46.1 (C, C-14), 47.0 (C, C-13), 49.3 (CH, C-5), 49.7 (CH, C-8), 50.0 (CH_2, C-12), 50.2 (CH, C-9), 55.4 (CH, C-17), 55.8 (CH, C-3), 62.0 (CH, C-20), 74.9 (CH_2, C-29), 78.3 (CH, C-16), 121.6 (CH, C-1), 137.2 (C, C-10), 156.4 (C, C-1′), 211.6 (C, C-11); ES-MS *m*/*z* 457.4 $[M + H]^+$ (100), 458.4 (5); HRES-MS *m*/*z* calcd for $C_{28}H_{45}N_2O_3$, 457.3430; found, 457.3470; Anal. ($C_{28}H_{44}N_2O_3$) C, H, N.

Biochemical Methods. In Vitro AChE Inhibition Assay. Enzymes *Ee*AChE from *electrophorus electricus* (reference C 2888), *b*AChE from bovine erythrocytes (reference C 5021), and human recombinant *h*AChE (reference C 1682) were purchased from Sigma. *Tc*AChE was purified from the electric organ tissue of *T. californica*, as described.[42,43]

Inhibition of AChE activity was determined by the spectroscopic method of Ellman et al.,[33] using acetylthiocholine iodide as substrate, in 96-well microtiter plates. All solutions were brought to room temperature prior to use. Aliquots of 200 μL of a solution containing 640 μL of 10 mM DTNB in 0.1 M sodium phosphate, pH 8.0, 19.2 mL of the same buffer, and 13 μL of a solution of AChE (100 U/mL) in water, were added to each well, followed by 2 μL of an aqueous solution of the inhibitor. The reaction was initiated by adding 20 μL of acetylthiocholine iodide (7.5 mM) to each well and was followed by monitoring the appearance of the thiolate dianion produced by reduction of DTNB at 412 nm for 120 s at 25 °C in a Molecular Devices Spectra Max 384 Plus plate reader. Each inhibitor was evaluated at several concentrations in the range of 10^{-9} to 2×10^{-5} M. Percentage inhibition was calculated relative to a control sample (DMSO), and IC_{50} values displayed represent the mean ± standard deviation for triplicate assays.

Kinetic Inhibition Studies. The determination of the type of inhibition of compounds **26a** and **34** was done by plotting the reciprocal of the rate of the reaction against the reciprocal of the substrate concentration as Lineweaver−Burk plot using, on a 96-well microtiter plate, a series of eight concentrations for the inhibitor (from 2000 to 15 nM by diluting by a factor 2) and eight for the acetylthiocholine substrate (from 6400 to 80 nM by diluting by a factor 2) obtained with a Beckman Biomek 3000 and Biomek NX robots. The kinetics were followed under the same conditions as in the above experiments.

In vitro BuChE Inhibition Assay. Enzyme *h*BuChE from human serum (reference C 9971) was purchased from Sigma. Inhibition of BuChE activity was determined by the spectroscopic method of Ellman et al.,[33] using butyrylthiocholine iodide as substrate, in 96-well microtiter plates. All solutions were brought to room temperature prior to use. Aliquots of 200 μL of a solution containing 640 μL of 10 mM DTNB in 0.1 M sodium phosphate, pH 8.0, 19.2 mL of the same buffer, and 13 μL of a solution of BuChE (100U/mL) in water were added to each well, followed by 2 μL of an aqueous solution of the inhibitor. The reaction was initiated by adding 20 μL of butyrylthiocholine iodide (7.5 mM) to each well, followed by monitoring the appearance of the thiolate dianion produced by reduction of DTNB at 412 nm for 120 s at 25 °C in a Molecular Devices Spectra Max 384 Plus plate reader. Each inhibitor was evaluated at several concentrations in the range of 10^{-9} to 2×10^{-5} M. Percentage inhibition was calculated relative to a control sample, and IC_{50} values displayed represent the mean ± standard deviation for triplicate assays.

Computer-Aided Molecular Modeling. Calculations of molecules, the different superpositions and the various representations of molecules and docking were performed using sybyl software from Tripos (mmff 94 as force field, MOPAC for semiempirical calculations).

The molecular dynamics computations were carried out with the Discover module of the Accelrys software and the Cff91 forcefield.[44] We used the 2 Å resolution X-ray crystal structure of AChE of *Torpedo californica* complexed with decamethonium (PDB access code 1acl[37]). Throughout the simulations, the protein backbone was held frozen, and its side chains and the inhibitor were relaxed. Manual docking, followed by a preliminary round of energy-minimization (EM), was performed by use of our computer graphics facilities prior to molecular dynamics. The latter used the same protocol as in ref 41.[45] After 5000 fs initialization steps at 300 K, 100 steps of molecular dynamics (MD) were performed. These were done at 300 K during 5000 steps of 1 fs. Each snapshot was subjected to conjugate gradient energy minimization and stored. The search for the best conformation of the uncomplexed protein and inhibitors was carried out by the same protocol. Solvation energies of the selected minima were computed using the Poisson−Boltzmann (PB) procedure with the Delphi software (Table 4).[46] The solute and solvent dielectric constants were 4 and 80, respectively.

E_{tot} denotes the energy of the protein−ligand complex. δE_{lig} denotes the lowest energy of the isolated ligand following the above-mentioned MD and EM protocols. Similarly, E_{prot} denotes the lowest energy of the isolated protein using this protocol. δE_1 is the difference between E_{tot} and the sum of E_{prot} and E_{lig}. $E_{solvtot}$ is the PB solvation energy of the protein−ligand complex, while $E_{solvprot}$ and $E_{solvliig}$ are the corresponding solvation energies of the isolated protein and ligand, respectively. δE_2 is the difference between $E_{solvtot}$ and the sum of $E_{solvprot}$ and $E_{solvliig}$. E_{prot}: −10380.6; $E_{solvprot}$: −1591.8.

X-ray Crystallography. X-ray Structure Analysis of Compound 1.[47] Data were obtained from a small colorless prismatic crystal (0.50 × 0.35 × 0.17 mm). Empirical formula: C30H48N2O3, $M_w = 484.70$. The compound crystallizes in the triclinic system, space group *P*1, chiral, with one molecule in the unit-cell of parameters $a = 6.135(2)$, $b = 6.770(3)$, $c = 17.170(7)$ Å, $\alpha = 92.30(3)$, $\beta = 97.87$ (3), $\gamma = 99.35(3)°$, $V = 695.6$ Å;^{3} dc = 1.157 g cm^{-3}, $F(000) = 266$, λ (Mo Kα) = 0.710 73 Å, and $\mu = 0.074$ mm^{-1}. Data were measured with a Nonius Kappa-CCD area-detector diffractometer, using graphite monochromated Mo Kα radiation, according to the phi and omega scan method, up to $\theta = 27.0°$. A total of 6626 intensity data was collected and reduced to 4963 unique triclinic reflections ($R_{int} = 0.025$).[48] Structure was solved with program SHELXS86[49] and refined by full-matrix least-squares, upon all unique F^2 with program SHELXL97.[50] All the hydrogen atoms were located in difference Fourier syntheses and fitted at theoretical positions. They were assigned an isotropic displacement parameter equivalent to 1.12 the one of the bonded atom, 1.15 for those of the methyl groups and treated as riding.

Refinement of 328 parameters converged to $R1(F) = 0.0501$ calculated with the 4448 observed reflections having $I \geq 2\sigma(I)$ and $wR2(F^2) = 0.1419$ calculated with all the 4963 unique data. Goodness-of-fit was 1.024. The residual electron density was found between −0.18 and 0.20 eÅ^{-3}. Crystallographic results are given in the cif file and Supporting Information.

Molecular Conformation. The structure has been elucidated unambiguously by the X-ray structure analysis. The molecule is shown in Figure 1, with the known absolute configuration of steroid compounds and the conventional labeling, drawn with program *PLATON*.[51] The chain fixed at C17 is stabilized by an intramolecular hydrogen bond of 2.973 Å established between the hydroxyl group OH16 and the nitrogen N**B**. All ring conformations can be deduced from torsion angles values. So, the new ring including atom O1′ is in an envelope conformation in C4, this atom being deviated by 0.720(2) Å from the mean plane of the other five atoms. As a consequence of the double bond C1−C10 of 1.336(3) Å, ring A appears nearly in a half-chair conformation with atoms C3 and C4 deviated, respectively, by −0.268 (2) and 0.527(2) Å from the mean plane of the other four atoms. Ring B exhibits the chair conformation of the cycloheptane, with atoms C5 and C10, respectively, situated at −1.234(2) and −0.961(2) Å, and atom C8 at 0.701(2), from the central mean plane of the four other atoms (C6, C7, C9, C19). Ring C can be seen as a flattened chair in C9, atoms C9 and C13 being deviated by, respectively, −0.369(2) and 0.717(2) Å from the mean plane of the other four atoms of this ring. Cycle D exhibits a nearly half-chair conformation, with the atoms C13 and C14 apart by 0.289(2) and −0.486(2) Å from the mean plane of the remaining atoms. In the crystal packing, only Van der Waals contacts are observed.

Acknowledgment. We thank the CNRS and ICSN for financial support. T. Sauvaitre and M. Barlier were supported by fellowhips from the Institut de Chimie des Substances Naturelles (ICSN-CNRS). Professor J. L. Lallemand is gratefully acknowledged for his interest in our work, as well as Dr. Françoise Guéritte and Alain Montagnac, responsible for the natural products and chemical libraries of ICSN. We would also like to thank Dr. Françoise Kuong-Huu and Dr. Jordi Molgo for fruitful discussions and R. H. Dodd for carefully reading the manuscript and for helpful comments. The molecular dynamics computations were performed on the computers of CINES (Montpellier, France), which we thank for support. We also wish to thank Dr. Jean-Edouard Ombetta (Faculte de Pharmacie de Tours, France) for his help in the Delphi computations.

Supporting Information Available: Detailed experimental procedures, compound characterization data for **7a**−**7i**, **8b**−**8i**, **9a**−**9i**, **10**−**19**, **20a**−**26b**, and **27**−**33** and crystal data and structure refinement for compound **1**. This material is available free of charge via the Internet at http://pubs.acs.org.

References

(1) Walsh, D. M.; Selkoe, D. J. Deciphering the molecular basis of memory failure in Alzheimer's disease. *Neuron* **2004**, *44*, 181−193.
(2) Hardy, J.; Selkoe, D. J. The amyloid hypothesis of Alzheimer's disease: Progress and problems on the road to therapeutics. *Science* **2002**, *297*, 353−356.
(3) Tolnay, M.; Probst, A. Review: tau protein pathology in Alzheimer disease and related disorders. *Neuropathol. Appl. Neurobiol.* **1999**, *25*, 171−187.
(4) (a) Bartus, R. T.; Dean, R. L., 3rd; Beer, B.; Lippa, A. S. The cholinergic hypothesis of geriatric memory dysfunction. *Science* **1982**, *217*, 408−414. (b) Dunnett, S. B.; Fibiger, H. C. Role of forebrain cholinergic system in learning and memory: relevance to the cognitive deficits of aging and Alzheimer's dementia. *Prog. Brain Res.* **1993**, *98*, 413−420. (c) Bartus, R. T. On neurodegenerative diseases, models and treatment strategies: Lessons learned and lessons forgotten a generation following the cholinergic hypothesis. *Exp. Neurol.* **2000**, *163*, 495−529.
(5) Sugimoto, H. Donepezil hydrochloride: A treatment drug for Alzheimer's disease. *Chem. Rec.* **2001**, *1*, 63−73.
(6) Jann, M. W. Rivastigmine, a new-generation cholinesterase inhibitor for the treatment of Alzheimer's disease. *Pharmacotherapy* **2000**, *20*, 1−12.
(7) (a) Marco-Contelles, J.; Carreiras, M. d. C.; Rodriguez, C.; Villarroya, M.; Garcia, A. G. Synthesis and pharmacology of Galantamine. *Chem. Rev.* **2006**, *106*, 116−133. (b) Robinson, D. M.; Plosker, G. L. Galantamine extended release. *CNS Drugs* **2006**, *20*, 673−681.
(8) Rogawski, M. A.; Wenk, G. L. The neuropharmacological basis for the use of memantine in the treatment of Alzheimer's disease. *CNS Drug Rev.* **2003**, *9*, 275−308.
(9) Soreq, H.; Seidman, S. Acetylcholinesterase: New roles for an old actor. *Nat. Rev. Neurosci.* **2001**, *2*, 8−17.
(10) Silman, I.; Sussman, J. L. Acetylcholinesterase: Classical and nonclassical functions and pharmacology. *Curr. Opin. Pharmacol.* **2005**, *5*, 1−10.
(11) Johnson, G.; Moore, S. W. The adhesion function on acetylcholinesterase is located at the peripheral anionic site. *Biochem. Biophys. Res. Commun.* **1999**, *258*, 758−762.
(12) Giacobini, E. Cholinesterase: New roles in brain function and Alzheimer's disease. *Neurochem. Res.* **2003**, *25*, 512−522.
(13) Blasina, M. F.; Faria, A. C; Gardino, P. F.; Hokoc, J. N.; Almeida, O. M.; de Mello, F. G.; Arruti, C.; Dajas, F. Evidence of non-cholinergic function of acetylcholinesterase during development of chicken retina as shown by fasciculin. *Cell Tissue Res.* **2000**, *299*, 173−174.
(14) Munoz, F. J.; Aldunate, R.; inestrosa, N. C. Peripheral binding site is involved in the neurotrophic activity of acetylcholinesterase. *NeuroReport* **1999**, *26*, 3621−3625.
(15) Sharma, K. V.; Koenigsberger, C.; Brimijoin, S.; Gigbee, J. W. Direct evidence for an adhesive function in the noncholinergic role of acetylcholinesterase in neurite outgrowth. *J. Neurosci. Res.* **2001**, *63*, 165−175.
(16) Inestrosa, N. C.; Alarcon, R. Molecular interactions of acetylcholinesterase with senile plaques. *J. Physiol. (Paris)* **1998**, *92*, 314−344.
(17) (a) Inestrosa, N. C; Alvarez, A.; Calderon, F. Acetylcholienesterase is a senile plaque component that promotes assembly of amyloid β-peptide into Alzheimer's filaments. *Mol. Psychiatry* **1996**, *1*, 359−361. (b) De Ferrari, G. V.; Canales, M. A; Shin, I.; Weiner, L. V.; Silman, I.; Inestrosa, N. C. A structural motif that promotes amyloid β-peptide fibril formation. *Biochemistry* **2001**, *40*, 10447−10457.
(18) De Ferrari, G. V.; Canales, M. A.; Shin, I.; Weiner, L. M.; Silman, I.; Inestrosa, N. C. A structural motif of acetylcholinesterase that promotes amyloid β-peptide fibril formation. *Biochemistry* **2001**, *40*, 10447−10457.
(19) Bartolini, M.; Bertucci, C.; Cavrini, C.; Andrisano, V. β-Amyloid aggregation induced by human cholinesterase: Inhibition studies. *Biochem. Pharmacol.* **2003**, *65*, 407−416.
(20) (a) Mary, A.; Renko, D. Z.; Guillou, C.; Thal, C. Potent acetylcholinesterase inhibitors: Design, synthesis and structure−activity relationships of galanthamine bis-ligands. *Bioorg. Med. Chem.* **1998**, *6*, 1835−1850. (b) Guillou, C.; Mary, A.; Renko, D. Z.; Gras, E.; Thal, C. Potent acetylcholinesterase inhibitors: Design, synthesis and structure−activity relationships of alkylene linked bis-galanthamine and galanthaminium salts. *Bioorg. Med. Chem. Letters* **2000**, *10*, 637−639. (c) Greenblatt, H. M.; Guillou, C.; Guenard, D., Argaman, A.; Botti, S.; Badet, B.; Thal, C.; Silman, I.; Sussman; J. L. The complex of a bivalent derivative of galanthamine with Torpedo acetylcholinesterase displays drastic deformation of the active-site gorge: Implications for structure-based drug design. *J. Am. Chem. Soc.* **2004**, *126*, 15405−15411.
(21) Vincent, D.; Mathou, T. Inhibiting action of boxwood (*Buxus sempervirens* and *Buxus balearica*) on the cholinesterase of serum. *C. R. Hebd. Seances Acad. Sci.* **1945**, *220*, 474−476.
(22) Vincent, D.; Sero, I.; Laurent, R. Données pharmacologiques sur le buis. *Therapie* **1948**, *3*, 29−32.
(23) (a) Choudhary, M. I.; Shahnaz, S.; Parveen, S.; Khalid, A.; Ayatollahi, S. A. M.; Atta-ur-Rahman; Parvez, M. New triterpenoid alkaloid cholinesterase inhibitors from *Buxus hyrcana*. *J. Nat. Prod.* **2003**, *66*, 739−742. (b) Atta-ur-Rahman; Parveen, S.; Khalid, A.; Farooq, A.; Ayatollahi, S. A. M.; Choudhary, M. I. Acetylcholinesterase inhibiting triterpenoidal alkaloids from *Buxus hyrcana*. *Heterocycles* **1998**, *49*, 481−488.
(24) Atta-ur-Rahman Parveen, S.; Khalid, A.; Farooq, A.; Choudhary, M. I. Acetyl and butyrylcholinesterase-inhibiting triterpenoids from *Buxus papillosa*. *Phytochemistry* **2001**, *58*, 963−968.
(25) Atta-ur-Rahman; Zaheer ul, H.; Feroz, F.; Khalid, A.; Nawaz, S. A.; Khan, M. R.; Choudhary, M. I. Cholinesterase-inhibiting new steroidal alkaloids from *Sarcococca hookeriana* of Nepalese origin. *Helv. Chim. Acta* **2004**, *87*, 439−448.

(26) Atta-ur-Rahman; Feroz, F.; Zaheer ul, H.; Nawaz, S. A.; Khan, M. R.; Choudhary, M. I. New steroidal alkaloids from sarcococca. *Nat. Prod. Res.* **2003**, *17*, 235−241.
(27) Kalauni, S. K.; Choudhary, M. I.; Khalid, A.; Manandhar, M. D.; Shaheen, F.; Atta-ur-Rahman; Gewali, M. B. New cholinesterase inhibiting steroidal alkaloids from the leaves of *Sarcococca coriacea* of Nepalese origin. *Chem. Pharm. Bull.* **2002**, *50*, 1423−1426.
(28) Herlem, D. *Thèse: Alkaloids from Buxus balearica* Willd (Buxacées)− Isolation and structural determination; Science Faculty of Paris: Paris, 1967.
(29) Compound **1** has been previously prepared by pyrolysis at 210 °C under 0.01 mmHg in the presence of tetramethylammonium hydroxide. Herlem-Gaulier, D.; Kuong-Huu-Lainé, F.; Goutarel, R.; Magdeleine, M. J. Alcaloïdes stéroïdiques LXXII. Alcaloïdes du groupe des cylcloxobuxidines retirés du *Buxus balearica* Willd: *N*-3-*iso*-Butyryl cycloxobuxidine-F (baléabuxidine), *N*-3-isobutyryl cycloxobuxidine-H, N-3-benzoyl cycloxobuxidine-F et cycloxobuxoxazine-C. *Bull. Soc. Chim. Fr.* **1968**, *2*, 763−773.
(30) Shaw, J. T.; Corbett, W. L.; Layman, D. L.; Cuny, G. D.; Kerschner, J. Fused s-triazino heterocycles. XV. 13*H*-4,6,7,13a,13c-pentaazabenzo[*hi*]chrysene, 13*H*,4,7,13a,13c- tetraazabenzo [*hi*]chrysene and 7*H*-3,7,10,10b-tetraazacyclohepta[*de*]naphtalene, three new ring systems *J. Heterocycl. Chem.* **1988**, *25*, 1837−1840.
(31) Mary, A.; Zafiarisoa, D.; Guillou, C.; Thal, C. Selective N-demethylation of galanthamine via a nonclassical Polonovski reaction. *Tetrahedron Lett.* **1997**, *38*, 5151−5152.
(32) Ellman, G. L.; Courtney, K. D.; Andres, V.; Featherstone, R. M. A new and rapid colorimetric determination of acetylcholinesterase activity. *Biochem. Pharmacol.* **1961**, *7*, 88−95.
(33) Giacobini, E. *Butyrylcholinesterase its functions and inhibitors*; Martin Dunitz: 2003.
(34) Kuhl D. E.; Koeppe R. A.; Snyder, S. E.; Minoshima, S., Frey, K. A.; Kilbourn, M. R. *Ann. Neurol.* **2006**, *59*, 13−20.
(35) Khalid, A.; Zaheer-ul-Haq Anjum, S.; Riaz Khan, M.; Atta-ur-Rahman, Choudhary, M. I. Kinetic and structure−activity relationship studies on pregnane-type steroidal alkaloids that inhibit cholinesterases. *Bioorg. Med. Chem.* **2004**, *12*, 1995−2003.
(36) Robaire, B.; Kato, G. Effect of edrophonium, eserine, decamethonium, D-tubocurarine, and gallamine on the kinetics of membrane-bound and solubilized Eel acetylcholinesterase. *Mol. Pharmacol.* **1975**, *11*, 722−734.
(37) Harel, M.; Schalk, I.; Ehret-Sabattier, L.; Bouet, F.; Goeldner, M.; Hirth, C.; Axelsen, P.; Silman, I.; Sussman, J. L. Quaternary ligand binding to aromatic residues in the active-site gorge of acetylcholinesterase. *Proc. Nat. Acad. Sci. U.S.A.* **1993**, *90*, 9031−9035.
(38) Khalid, A.; Azim, M. K.; Parveen, S.; Atta-ur-Rahman, Choudhary, M. I. Structural basis of acetylcholinesterase inhibition by triterpenoidal alkaloids. *Biochem. Biophys. Res. Comm.* **2005**, *331*, 1528−32.
(39) For a recent application, see: Roux, C.; Gresh, N.; Perera, L. E.; Piquemal, J.-P.; Salmon, L. Binding of 5-phospho-D-arabinonohydroxamate and 5-phospho-D-arabinonate inhibitors to zinc phosphomannose isomerase from *Candida albicans* studied by polarizable molecular mechanics and quantum mechanics. *J. Comput. Chem.* **2007**, *28*, 938−957.
(40) Wu, H. J.; Roux, B. Calculation of absolute protein−ligand binding free energy from computer simulation. *Proc. Natl. Acad. Sci. U.S.A.* **2005**, *102*, 6825−6830.
(41) (a) Chipot, C.; Pearlman, D. A. Free energy calculations. The long and winding gilded road. *Mol. Simul.* **2002**, *28*, 1−12. (b) Chipot, C.; Rozanska, X.; Dixit, S. B. Can free energy calculations be fast and accurate at the same time? Binding of low-affinity, nonpeptide inhibitors to the SH2 domain of the src protein. *J. Comp.-Aided Mol. Des*. **2005**, *19*, 765−770.
(42) Raves, M. L.; Harel, M.; Pang, Y. P.; Silman, I.; Kozikowski, A. P.; Sussman, J. L. 3D structure of acetylcholinesterase complexed with the nootropic alkaloid, (−)-huperzine A. *Nat. Struct. Biol.* **1997**, *4*, 57−63.
(43) Sussman, J. L.; Harel, M.; Frolow, F.; Varon, L.; Toker, L.; Futerman, A. H.; Silman, I., Purification and crystallization of a dimeric form of acetylcholinesterase from *Torpedo californica* subsequent to solubilization with phosphatidylinositol-specific phospholipase C. *J. Mol. Biol.* **1988**, *203*, 821−823.
(44) *Accelrys Inc.*, 9685 Scranton Rd., San Diego, CA 92121−3752.
(45) Plocki, S.; Tavarès-Camarinha, F.; Ahamada-Himidi, A.; Aoun, D.; Dong, C. Z.; Massicot, F.; Huet, J.; Adolphe-Pierre, S.; Chau, F.; Ombetta, J. E.; Gresh, N.; Godfroid, J. J.; Heymans, F. Inhibition of secretory phospholipase A2. Molecular modeling, design, and synthesis of less lipophilic derivatives of 4,5-dihydro-3-(4-tetradecyloxybenzyl)-1,2,4*H* oxadiazol-5-one specific for group II enzyme. *Eur. J. Org. Chem*. **2005**, 2747−2757.
(46) Honig, B.; Sharp, K.; Yang, A. S. Macroscopic models of aqueous solutions: Biological and chemical applications. *J. Phys. Chem.* **1993**, *97*, 1101−1109.
(47) CCDC 651096 contains the Supplementary Crystallographic data for compound **1**. These data can be obtained free of charge via www.ccdc.cam.ac.uk or from the Cambridge Crystallographic Data Centre, 12 Union Road, Cambridge CB2 1EZ, U.K. (fax: +44-(0)1223−336033, E-mail: deposit@ccdc. cam. ac.uk).
(48) Otwinowski, Z.; Minor, W. Processing of X-ray Diffraction Data Collected in Oscillation Model, Methods in Enzymology, Volume 276: Macromolecular Crystallography, part A; Carter, C. W., Jr., Sweet, R. M., Eds.; Academic Press: New York, 1997; pp 307−326.
(49) Sheldrick, G. M. *SHELXS86. Acta Cryst*. *A* **1990**, *46*, 467−473.
(50) Sheldrick, G. M. *SHELX97*, Program for the Refinement of Crystal Structures; Univ. of Göttingen: Germany, 1997.
(51) (a) Spek, A. L.; *Platon*, A multipurpose crystallographic tool; Utrecht University: Utrecht, The Netherlands. (b) Spek, A. L. Single-crystal structure validation with the program Platon. *J. Appl. Cryst.* **2003**, *36*, 7−13.

JM070536W